Digital quantum simulation of bosonic systems and quantum complementarity

Victor P. Brasil[1,*] Diego S. Starke[1,†] and Jonas Maziero[1,‡]

[1] *Physics Department, Center for Natural and Exact Sciences, Federal University of Santa Maria, Roraima Avenue 1000, Santa Maria, RS, 97105-900, Brazil*

(Dated: March 25, 2025)

Digital quantum simulation has emerged as a powerful approach to investigate complex quantum systems using digital quantum computers. Many-particle bosonic systems and intricate optical experimental setups pose significant challenges for classical simulation methods. Utilizing a recently developed formalism that maps bosonic operators to Pauli operators via the Gray code, we digitally simulate interferometric variants of Afshar's experiment on IBM's quantum computers. We investigate the analogous experiments of Unruh and Pessoa Júnior, exploring discussions on the apparent violation of Bohr's complementarity principle when considering the entire experimental setup. Furthermore, we analyze these experiments within the framework of an updated quantum complementarity principle, which applies to specific quantum state preparations and remains consistent with the foundational principles of quantum mechanics. Our quantum computer demonstration results are in good agreement with the theoretical predictions and underscore the potential of quantum computers as effective simulators for bosonic systems.

Keywords: Digital quantum simulation, Afshar's experiment, Unruh's experiment, Bohr's complementarity principle, Quantum complementarity relations

I. INTRODUCTION

Feynman [1] proposed that quantum systems could be used to simulate other quantum systems. This proposal is capable of addressing the limitations inherent in classical computational methods for quantum system simulation, especially concerning the exponential increase in parameters necessary for describing such systems. Today, it is understood that quantum systems can be simulated using quantum devices designed for specific problem-driven evolutions [2]. Lloyd [3] expanded on this idea by establishing the theoretical foundation of quantum computers as universal machines capable of addressing a broad range of problems. These devices leverage quantum phenomena such as superposition and entanglement to solve both classical and quantum problems more efficiently than classical computers [4, 5]. However, realizing this potential requires effective methods for mapping problems onto quantum computers, a task that is generally difficult.

A significant challenge in the mapping process lies in the simulation of bosonic systems [6–8]. These systems are characterized by an infinite-dimensional Hilbert space, necessitating a two-step simulation approach [6]: *i*) encoding bosonic states into qubit states, and *ii*) establishing an isomorphic mapping of bosonic field operators to linear operators within the qubit state space. Following this framework, Mohan *et al.* [9] adopted a methodology guided by Refs. [10, 11], utilizing the Gray code to map bosonic operators to Pauli operators. This approach enabled the construction of a quantum circuit capable of simulating a beam splitter. To demonstrate the effectiveness of this formalism, Mohan *et al.* implemented the Hong-Ou-Mandel interference experiment.

The investigation of bosonic systems holds significant importance across numerous research domains, including biology [12–15], chemistry on bosonic devices (a promising model of quantum computation) [16–19], condensed matter physics [20–24] and quantum optics [25–28]. Our study aims in particular to simulate bosonic systems as a means to explore the fundamentals of quantum mechanics, building upon the framework outlined in Ref. [9]. Thus, we have access to digital quantum simulations capable of replicating the experimental setup analogous to the modified double-slit experiment conducted by Afshar *et al.* [29]. Afshar's experiment suggests that it is possible to observe both aspects of wave-particle duality at the same experimental setup, thereby asserting a breach of Bohr's complementarity principle. Building upon this idea, a modified version of Unruh's experiment [30] is considered, followed by an extended experimental configuration, Pessoa Júnior's experiment [31]. The goal is to explore the formalism presented by Mohan *et al.* and its applicability to advanced experimental configurations, such as those proposed in Pessoa Júnior's experiment. It is worthwhile mentioning that while the modified Unruh's experiment can be simulated with

*Electronic address: victor.brasil@acad.ufsm.br
†Electronic address: starkediego@gmail.com
‡Electronic address: jonas.maziero@ufsm.br

a single qubit, the formalism is extended to simulate Pessoa Júnior's experiment. To the best of our knowledge, mapping Pessoa Júnior's setup for simulation on quantum computers is a nontrivial task, making this implementation a notable contribution of this article.

The organization of this paper is as follows. In Section II A, the formalism introduced by Mohan *et al.* is revisited. Section II B reviews the quantum complementarity principle (QCP), Afshar's experiment, and the arguments that Afshar used to claim the violation of BCP. Sections II C and II D explore different versions of nested MZI as described by Pessoa Júnior in Ref. [31] as an analogous version of Afshar's experiment. Sections II C 1 and II D 1 detail the quantum digital simulation of these experiments. In Section II E, the results are analyzed employing QCP. Final remarks are presented in Sec. III. The demonstrative results compiled in this study to develop the histograms and the plots are available in Ref. [32].

II. DIGITAL QUANTUM SIMULATION OF INTERFEROMETRIC VERSIONS OF AFSHAR'S EXPERIMENT AND THE QUANTUM COMPLEMENTARITY PRINCIPLE

A. Formalism for digital quantum simulation of bosonic systems

To illustrate the method constructed by Mohan *et al.* in Ref. [9], let us first consider a BS - where the reflected beam picks up a phase of $\pi/2$ - depicted in Fig. 1, with two input modes, A and B, and two output modes, C and D. Boson annihilation operators are denoted by lowercase letters a, b, c, and d, corresponding to the respective uppercase letter modes. The general unitary transformation for a lossless BS is represented by [33]

$$U_{\rm BS} = \exp\{i\theta(b^\dagger a + b a^\dagger)\}, \tag{1}$$

where $\theta = \arctan(R/T)$ relates to the ratio between the reflection R and transmission T coefficients. In subsequent analysis of specific cases where $T \neq R$, we explicitly denote this optical element by BBS (biased beam splitter).

The relations between input and output modes annihilation and creation operators are expressed by [33]

$$\begin{aligned} c &= Ta + iRb, \qquad d = iRa + Tb, \\ c^\dagger &= Ta^\dagger - iRb^\dagger, \quad d^\dagger = -iRa^\dagger + Tb^\dagger, \end{aligned} \tag{2}$$

and conversely

$$\begin{aligned} a &= Tc - iRd, \qquad b = -iRc + Td, \\ a^\dagger &= Tc^\dagger + iRd^\dagger, \quad b^\dagger = iRc^\dagger + Td^\dagger. \end{aligned} \tag{3}$$

These relations are derived in App. A.

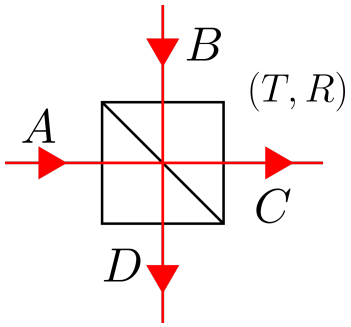

Figure 1: Beam splitter with input modes A and B and output modes C and D, characterized by transmission and reflection coefficients T and R, respectively. Each reflection adds a phase of $\pi/2$ to the reflected beam.

In Quantum Mechanics (QM) second quantization, the states of quantum systems (quantons) are usually described by state vectors in a Fock space $\mathscr{F}$, a natural framework for dealing with systems of indistinguishable particles [34]. In general, a Fock state of a system with N particles can be represented by

$$|n_1, n_2, \cdots, n_m, \cdots\rangle \in \mathscr{F}_N, \tag{4}$$

where the first mode is occupied by n_1 photons, the second by n_2 photons, and so on (with the constraint that $\sum_j n_j = N$), and $\mathscr{F}_N$ is the N-particle subspace of $\mathscr{F}$. The general state vector of this system is a linear superposition

of these states:

$$|\psi\rangle = \sum_{n_1}\sum_{n_2}\cdots\sum_{n_m}\cdots C_{n_1,n_2,\cdots,n_m,\cdots}|n_1,n_2,\cdots,n_m,\cdots\rangle,$$

with $C_{n_1,n_2,\cdots,n_m,\cdots}\in\mathbb{C}$. The authors in Ref. [9] began by encoding each Fock state into a qubit state using the Gray code. The number of qubits N_q needed to simulate the system depends on the total number of photons, N, and the number of modes, m, through the relation $N = m(2^{N_q}-1)$.

Adjacent numbers in Gray code have a Hamming distance equal to one and can be easily converted to binary code while maintaining the same number of digits. A method of conversion between the two representations is achieved by considering the general binary code as $B_1B_2\cdots B_{N_q-1}B_{N_q}$, where B_1 and B_{N_q} are the most significant and least significant digits, respectively. The same is valid for a general Gray code represented as $G_1G_2\cdots G_{N_q-1}G_{N_q}$. The most significant digit in the two representations is the same, i.e., $G_1 = B_1$, and the subsequent digits of the Gray code are obtained in descending order of significance by the recurrence formula

$$G_k = B_k \oplus B_{k-1}, \tag{5}$$

where the symbol $\oplus$ denotes the "exclusive or" operation. Two (j-mode) sequential Fock states in Gray code notation can be represented as

$$|0_1,\cdots,n_j,\cdots,0_m,\cdots\rangle_F \;\mapsto\; |0^{\otimes N_q}\rangle_1\otimes\cdots\otimes\left|G_1\cdots G_{k-1}G_kG_{k+1}\cdots G_{N_q}\right\rangle_j\otimes\cdots\otimes|0^{\otimes N_q}\rangle_m, \tag{6}$$

$$|0_1,\cdots,n_j-1,\cdots,0_m,\cdots\rangle_F \;\mapsto\; |0^{\otimes N_q}\rangle_1\otimes\cdots\otimes\left|G_1\cdots G_{k-1}G'_kG_{k+1}\cdots G_{N_q}\right\rangle_j\otimes\cdots\otimes|0^{\otimes N_q}\rangle_m. \tag{7}$$

Due to the Hamming distance between consecutive states being equal to one, they vary by just one bit (in this case, $G_k \neq G'_k$). The bosonic operators act on these states as follows:

$$x_{n_j}|n_1,\cdots,n_j,\cdots,n_m,\cdots\rangle = \sqrt{n_j}\;|n_1,\cdots,n_j-1,\cdots,n_m,\cdots\rangle, \tag{8}$$

$$x^\dagger_{n_j}|n_1,\cdots,n_j-1,\cdots,n_m,\cdots\rangle = \sqrt{n_j}\;|n_1,\cdots,n_j,\cdots,n_m,\cdots\rangle. \tag{9}$$

The map between operators is constructed by analyzing which bit is flipped in each state transition and then acting a spin ladder operator ($\mathcal{Q}_{G_k}$) in the qubit of the corresponding position k:

$$x_{n_j} \;\mapsto\; \mathbb{I}^{\otimes N_q}\otimes\cdots\otimes\left(\mathcal{P}_{G_1}\otimes\cdots\otimes\mathcal{P}_{G_{k-1}}\otimes\mathcal{Q}_{G_k}\otimes\mathcal{P}_{G_{k+1}}\otimes\cdots\otimes\mathcal{P}_{G_{N_q}}\right)_j\otimes\cdots\otimes\mathbb{I}^{\otimes N_q}, \tag{10}$$

$$x^\dagger_{n_j} \;\mapsto\; \mathbb{I}^{\otimes N_q}\otimes\cdots\otimes\left(\mathcal{P}_{G_1}\otimes\cdots\otimes\mathcal{P}_{G_{k-1}}\otimes\mathcal{Q}^\dagger_{G_k}\otimes\mathcal{P}_{G_{k+1}}\otimes\cdots\otimes\mathcal{P}_{G_{N_q}}\right)_j\otimes\cdots\otimes\mathbb{I}^{\otimes N_q}, \tag{11}$$

where

$$\mathcal{P}_{G_k} = \begin{cases}\frac{1}{2}(\mathbb{I}+Z) = |0\rangle\langle 0|, & \text{if } G_k = 0\\ \frac{1}{2}(\mathbb{I}-Z) = |1\rangle\langle 1|, & \text{if } G_k = 1\end{cases}, \tag{12}$$

$$\mathcal{Q}_{G_k} = \begin{cases}\frac{1}{2}(X+iY) = |0\rangle\langle 1|, & \text{if } G_k = 1\\ \frac{1}{2}(X-iY) = |1\rangle\langle 0|, & \text{if } G_k = 0\end{cases}, \tag{13}$$

and $\{\mathbb{I},X,Y,Z\}$ are the usual Pauli matrices. The identity operator $\mathbb{I}$ was used in place of $\mathcal{P}_{G_k}$ in the qubits associated to the modes $k\neq j$ because x_{n_j} and $x^\dagger_{n_j}$ act on mode j independently of the occupation numbers n_k of the other modes; since the bit string that encodes each number n_k is in principle an unknown sequence of zero's and one's, the identity $\mathbb{I} = |0\rangle\langle 0| + |1\rangle\langle 1|$ is used to ensure that those occupation numbers don't change. The complete bosonic operator expressed in terms of Pauli operators can be formulated as

$$x_P = \sum_{n_j=1}^{N} x_{n_j} = x_1 + x_2 + \cdots + x_N, \tag{14}$$

$$x^\dagger_P = \sum_{n_j=1}^{N} x^\dagger_{n_j} = x^\dagger_1 + x^\dagger_2 + \cdots + x^\dagger_N. \tag{15}$$

B. Quantum complementarity and Afshar's experiment

Bohr's complementarity principle (BCP) [35] has long been a cornerstone for understanding QM. Until recently, the exact origin of BCP within QM remained unclear. However, Ref. [36] demonstrated that a quantum version of BCP can be derived directly from the foundational postulates of QM, offering a deeper theoretical basis for this principle.

The updated QCP proposed in Ref. [37] is stated as follows: *For a given quantum state preparation ρ_t at a specific time instant t, the wave-like and particle-like manifestations of a quanton are constrained by the quantum complementarity relation (QCR)*

$$\mathfrak{W}(\rho_t) + \mathfrak{P}(\rho_t) \leq \alpha(d), \tag{16}$$

which is derived directly from the axioms of QM, where $\mathfrak{W}$ is a quantifier of wave-like behavior, $\mathfrak{P}$ is a quantifier of particle-like behavior, and α is a constant that depends only on the dimension d of the quanton. Deriving QCRs of this type becomes achievable after taking into account quantum coherence [38] as a good quantifier of $\mathfrak{W}$ aligned with certain restrictions on quantum states ρ (density operator) provided by quantum theory. The procedure for obtaining QCRs shows that the QCP can be uniquely derived from the QM postulates. The subscript t in ρ_t denotes the quantum state at a precise instant of time that marks the unitary evolution of the system, implying that the quantum state plays a crucial role in analyzing wave-particle duality, as it clearly demonstrates that QCRs must be continuously evaluated as the state evolves over time. An example of QCR is [37]

$$C_{l_1}(\rho_t) + P_{l_1}(\rho_t) \leq d - 1. \tag{17}$$

Here, $\mathfrak{W}(\rho_t) = C_{l_1}(\rho_t) = \sum_{j\neq k} |\rho_{jk}|$ is known as the l_1-norm quantum coherence, where ρ_{jk} are the elements of the density operator ρ_t on a given basis and the predictability measure is given by $\mathfrak{P}(\rho_t) = P_{l_1}(\rho_t) = d-1-\sum_{j\neq k}\sqrt{\rho_{jj}\rho_{kk}}$. Equality is achieved when the analyzed system is pure.

The principle can be extended to evaluate quantum correlations between a bipartite quantum system by introducing the entanglement monotone $\mathfrak{E}(\rho_t)$. For a particular choice of $\mathfrak{W}(\rho_t)$, $\mathfrak{P}(\rho_t)$ in Eq. (16), which satisfy some basic properties [39, 40], it is always possible to establish a quantum complete complementarity relation given by $\mathfrak{W}(\rho_t) + \mathfrak{P}(\rho_t) + \mathfrak{E}(\rho_t) = \alpha(d)$, also known as the triality relation [41–45]. It is worth mentioning that although in this work we explore a single bosonic system, recent developments have been reported in Ref. [46] regarding the understanding of wave-particle duality as applied to many-body quantum systems involving both bosons and fermions.

Before the introduction of the QCP, the quantification of BCP was obtained through a complementarity relationship that can be expressed as

$$W + P \leq \beta \tag{18}$$

where β is a constant, W is the function that quantify the wave-like behavior, and P is the function that quantify the particle-like behavior. Quantifiers W and P can be flexibly chosen in different regions throughout the whole experimental setup. For example, for the MZI depicted in Fig. 2, let us consider that it is possible to adjust the transmission (T_1) and reflection (R_1) coefficients of the first biased beam splitter (BBS_1), where $T_1^2 + R_1^2 = 1$. Consider, for instance, that BBS_2 is a balanced beam splitter (BS), i.e., $T_2 = R_2 = 1/\sqrt{2}$. The objective is to infer the behavior of a quanton inside the MZI. One way of quantifying W, introduced in this context by Greenberger and Yasin [47], is through interferometric visibility $\mathcal{V}$, defined by the probabilities of detection p_i in a certain detector D_i ($i = 0, 1$) outside of MZI (after passing BS_2) as

$$\mathcal{V}_i = \frac{\max(p_i) - \min(p_i)}{\max(p_i) + \min(p_i)}. \tag{19}$$

Strictly speaking, it is possible to derive two expressions for $\mathcal{V}$, one for each of the detectors. The maximum and minimum probabilities arise for a different phase variation ϕ_{E}. So, the definition of interferometric visibility as a wave-like behavior quantifier lies in the phase sensitivity of probabilities outside the MZI, characterizing $\mathcal{V}$ as a wave-like behavior quantifier by retroinference. Predictability, which quantifies particle-like behavior, is frequently expressed as $\mathcal{P} = |T_1^2 - R_1^2|$. This quantifier can be understood as an *a priori* estimate, i.e., there will be more information about the photon's path when T_1 or R_1 is closer to 1, and less information when (T, R) have similar values, independently of the counts obtained after the experiment is completed. Thus, the complementarity relation is presented as $\mathcal{V}_i^2 + \mathcal{P}^2 = 1$, where $W = \mathcal{V}_i^2$, $P = \mathcal{P}^2$, and $\beta = 1$. It is worth to note that the construction of this kind of complementarity relation in the quantitative version of BCP is based on the *ad hoc* methods, i.e., the functions of W and P can be constructed in many ways and depend on the configuration of the experimental apparatus.

The quantum version of BCP proposed in Ref. [37] and the traditional way to examine BCP differ in many ways. The former has a background supported by QM and gave us a formal definition for quantifying the QCR. A violation

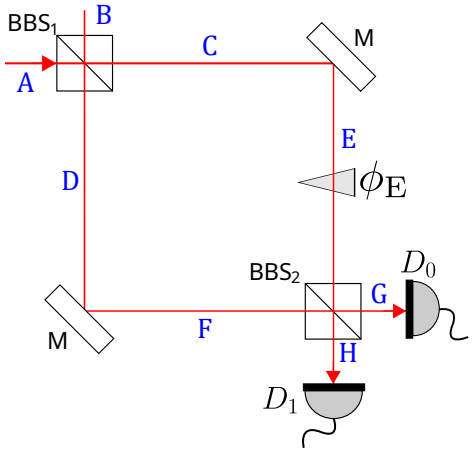

Figure 2: Mach-Zehnder interferometer composed of two BBSs. By utilizing a BBS_j (with $j = 0, 1$), the amplitudes of transmission (T_j) and reflection (R_j) – which specify the probability amplitudes of the quantons in each MZI arm - can be controlled. Mirrors (M) convert the horizontal (vertical) spatial mode into the vertical (horizontal) mode while introducing a global phase factor of $e^{i\pi/2}$; the phase shifter applies a phase factor of $e^{i\phi}$ to the vertical spatial mode, and D_0 and D_1 represent the detectors.

in this type of complementarity relation will reveal a fundamental issue with QM. In contrast, the latter still has a lack of conclusive formal definition, and there is a great flexibility in the construction of complementarity relations, being generally interested in the experimental apparatus as a whole along the lines of Bohr's intent. For the particular case of MZI discussed above with $BBS_2 = BS_2$, the QCP and the BCP agree in the complementarity behavior of the quanton, but disagree in many situations as delineated in Ref. [37]. In Sec. II E, the MZI in Fig. 2 will be explicitly analyzed in light of QCR, and the analysis will be related to two versions of Afshar's experiment proposed with nested MZIs.

In order to develop the *ad hoc* question and introduce Afshar's experiment, another case is discussed to highlight the lack of a clear formal definition of BCP as discussed in Ref. [48]. In Fig. 2, when the BBS_2 represents a beam splitter (BS_2) by setting $T_2 = R_2 = 1/\sqrt{2}$, the visibilities $\mathcal{V}_0$ and $\mathcal{V}_1$ are the same and the BCP remains valid and agrees with QCP. In Ref. [48] the authors examined a more general configuration of the MZI where it is possible to vary the coefficients T_2 and R_2 of the second BBS, and a lack of a formal definition for BCP becomes clearly evident. This choice is completely admissible because there is no restriction for this in the literature. This setup shows that $\mathcal{V}_0$ and $\mathcal{V}_1$ are no longer equal, leading to situations where the quantitative BCP can be violated, highlighting the shortcomings due to the absence of a formal definition of BCP and, in addition, showing that interferometric visibility is not, in general, a valid quantifier of W.

Afshar's experiment [29], depicted in Fig. 3, is a version of the double–slit experiment [49] that claims a violation of the BCP. Afshar used the *ad hoc* approach to the functions W and P combined with the lack of a clear definition of the BCP to construct a new complementarity relation in an attempt to understand the duality behavior in the double-slit experiment. The modified double-slit experiment is furnished with a wired grid depicted as black dots positioned in the s_2 plane. According to Afshar, the wire grid quantifies the maximum wave-like behavior through a non-destructive measurement, since the wires are positioned in regions of maximum destructive interference. Between the planes s_2 and s_3 there is a convex lens L that redirects the beams to the detectors D_A and D_B positioned in the s_3 plane. In an alternative experimental configuration, closing the slit A (B) results in only detector D_A (D_B) recording clicks. Afshar *et al.* carried out the experiment while maintaining the wire grid in place and verified that the correlation between the path and the detector is maintained, with a small number of photons triggering the opposite detector; however, the ultimate photon counts are significantly affected. Afshar concluded that this mechanism of relating path and detector holds even when both slits are open. For more discussions about this path retro-inference approach, see Ref. [50]. When neither slit is blocked, wave-like characteristics are observable at s_2 (where W reaches its peak) by the wire grid, and because only one detector will click for each photon, particle-like characteristics at s_3 denote the highest P. This scenario, according to Afshar, would represent a violation of the BCP, as there is a maximum W and a maximum P within the same experimental setup. It should be emphasized that there is extensive literature discussing Afshar's experiment [37, 50–59].

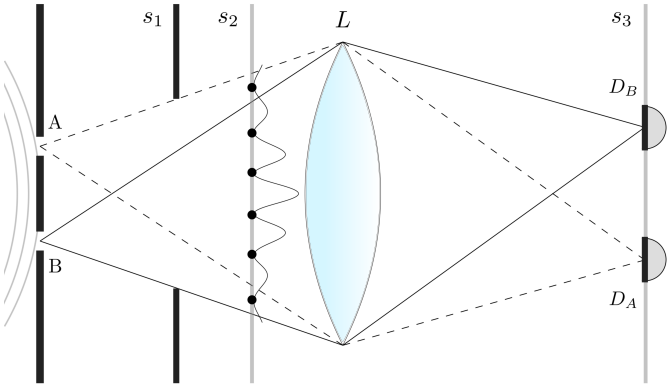

Figure 3: By modifying Young experiment and the methods of quantifying the wave- and particle-like behaviors of the quantons, Afshar claimed a violation of BCP. After measuring the positions of dark fringes (maximum destructive interference) at the screen s_2, Afshar replaced this screen by very thin wire grid at the positions previously determined. According to Afshar, this procedure is proposed for quantifying the wave-like behavior in a non-destructive way by verifying that this process does not significantly affect the photon counts at s_3. The area s_3 encompasses two positions, specifically detector D_A and detector D_B, located beyond lens L, which direct the photons to these regions. In an auxiliary experiment, Afshar closes slit A (B) and verifies that only the corresponding detector D_A (D_B) clicks; he concluded that, with both slits open, the slit-detector relation is still valid. With this in mind, since a maximum wave-like behavior is captured by the wire grid and a maximum particle-like behavior is obtained by the slit-detector relation, the author concludes that the BCP is violated.

C. Modified Unruh's experiment

Unruh's experiment [30] was originally proposed as a two-level system analogy to Afshar's experiment to examine whether BCP is violated. More recently, Ref. [37] examined this experiment to demonstrate the applicability of the QCP and its effectiveness in addressing duality behavior through QCRs.

Pessoa Júnior's modified version of Unruh's experiment [31], depicted in Fig. 4, introduces two additional phase shifters: $\phi_{\rm E}$ in $\rm MZI_1$ and $\phi_{\rm H}$ in $\rm MZI_2$. His motivation for incorporating these phase shifts is to better align Unruh's interferometric experiment with the time-step analysis of Afshar's experiment. The original setup, depicted in Fig. 4, corresponds to the case where $\phi_{\rm E} = \phi_{\rm H} = 0$.

Although the modified Unruh experiment can be simulated using a single qubit, we employ the formalism introduced in Ref. [9] to present the setup explored in Sec. II D. A key advantage of this formalism is its ability to facilitate a clearer analysis of the role of blockers through quantum computer simulations.

As discussed in Sec.II B, Afshar employed an *ad hoc* approach to defining wave and particle properties in a double-slit experiment, claiming that his findings constituted a violation of the quantitative version of BCP. In the modified Unruh setup, $\rm MZI_2$ serves as an analog to the wire grid region in Afshar's experiment, where mode H represents the minima of the interference pattern, capturing wave behavior non-destructively.

In the absence of the blocker B_0, the state after $\rm BS_2$ exhibits complete destructive interference in mode H and fully constructive interference in mode G. Unruh noted that mode H corresponds to the dark fringes where the wires were placed in Afshar's experiment to probe wave behavior. Importantly, the presence or absence of blocker B_1 in mode H does not alter this wave behavior.

When B_1 is absent, selectively inserting B_0 into mode C or D allows one to associate a detection event at D_1 with a quanton traveling via the upper path (modes C and E) and a detection at D_0 with the lower path (modes D and F). Following Afshar's interpretation, a click at either detector in the absence of B_0 is taken as an indication of the quanton's path, suggesting maximal corpuscular behavior.

A key objection to this reasoning arises when B_1 is placed in mode H. In this case, the previous path-detector association (established by blocking C or D with B_0) is no longer valid, as the interference structure is altered. Afshar *et al.* conducted their experiment with the wire grid in place and observed that the opposed detector still registered approximately 0.5% of photons, preserving the path-detector relationship. This stands in stark contrast to Unruh's version, where the presence of B_1 completely disrupts the path-detector correlation.

Let us begin the formal analysis considering the phases $\phi_{\rm E}$ and $\phi_{\rm H}$. We consider the initial state $|\psi_0\rangle = |1_{\rm A}, 0_{\rm B}\rangle = |10\rangle_{\rm AB}$. After $\rm BS_1$, the state evolves to $|\psi_1\rangle = \frac{1}{\sqrt{2}}\big(|10\rangle_{\rm CD} + i\,|01\rangle_{\rm CD}\big)$. The mirrors (M) change the mode from horizontal (vertical) to vertical (horizontal) and add a phase of $e^{i\pi/2} = i$. The phase shifter adds a phase of $e^{i\phi_{\rm E}}$ when mode E is populated. The state after these two optical elements and $\rm BS_2$ produces $|\psi_2\rangle = -\left(\frac{e^{i\phi_{\rm E}}+1}{2}\right)|10\rangle_{\rm GH} +$

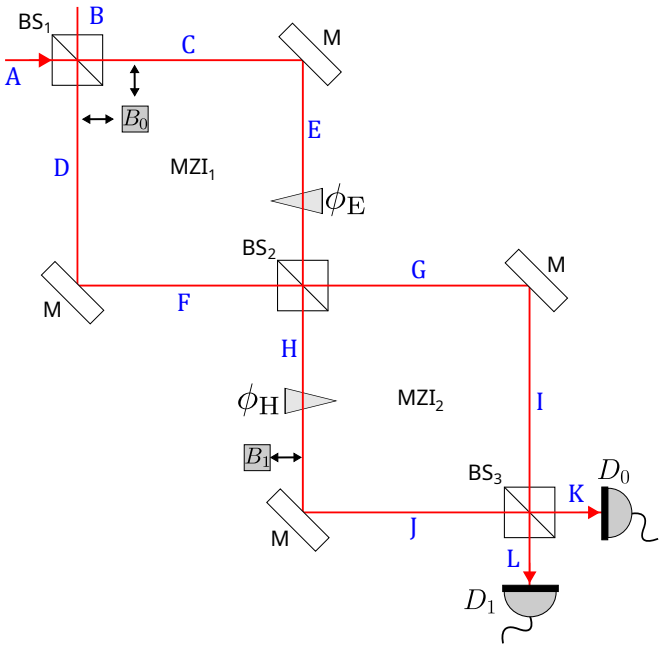

Figure 4: Modified Unruh's experiment proposed by Pessoa Júnior in Ref. [31]. The setup is composed of an extra MZI, namely MZI_2, inserted subsequently to the MZI_1 output modes. The main difference in this proposed version is choosing appropriate values for the phase shifts ϕ_E and ϕ_H to align Unruh's experiment with the original aim of Afshar's experiment. The boxes B_0 and B_1 represent the blockers that can be inserted into the quanton paths.

$i\left(\frac{e^{i\phi_\mathrm{E}}-1}{2}\right)|01\rangle_\mathrm{GH}$. Finally, after phase $e^{i\phi_\mathrm{H}}$, mirrors and BS_3, the state evolves to

$$|\psi_3\rangle = -\frac{1}{2\sqrt{2}}\left(e^{i\phi_\mathrm{E}}e^{i\phi_\mathrm{H}} - e^{i\phi_\mathrm{H}} - e^{i\phi_\mathrm{E}} - 1\right)|10\rangle_\mathrm{KL} - \frac{i}{2\sqrt{2}}\left(e^{i\phi_\mathrm{E}}e^{i\phi_\mathrm{H}} + e^{i\phi_\mathrm{E}} - e^{i\phi_\mathrm{H}} + 1\right)|01\rangle_\mathrm{KL}\,. \tag{20}$$

Pessoa Júnior explored the introduction of two phase shifts, ϕ_E and ϕ_H, selecting a specific case to demonstrate how it aligns more closely with Afshar's experiment. Since the Greenberger-Yasin formulation of the BCP does not impose explicit restrictions on the use of interferometric visibility, he follows the usual literature and assumes that Eq. (19) remains valid for MZI_1 even after BS_3.

According to Pessoa Júnior, in Afshar's experiment, one can examine different regions to interpret the quanton's behavior at each time step. Immediately after BS_1 (in MZI_1), the behavior is corpuscular. This notion, borrowed from the literature – particularly from experiments such as Wheeler's delayed choice [60] – suggests that a click in a detector following a photon's passage through the upper slit (upper arm of the MZI) or lower slit (lower arm of the MZI) implies that the photon originated from that specific path.

Inside MZI_2, the quanton's behavior is wave-like, as indicated by Eq. (19). This aligns with the role of the wire grid region in Afshar's experiment, where the wave nature of light is inferred. The phase settings that capture this sequence of behaviors in Pessoa Júnior's modified version of Unruh's experiment are $\phi_\mathrm{E} = \pi/2$ and $\phi_\mathrm{H} = 0$.

By keeping $\phi_\mathrm{H} = 0$ and varying ϕ_E, no wave behavior emerges through interferometric visibility, and only corpuscular behavior remains in MZI_1. The probabilities in Eq. (20) remain unchanged for different values of ϕ_E when $\phi_\mathrm{H} = 0$, characterizing a purely corpuscular behavior in MZI_1. Conversely, fixing $\phi_\mathrm{E} = \pi/2$ while varying ϕ_H maximizes the wave behavior in MZI_2, as inferred from the interferometric visibility. In this case, for $\phi_\mathrm{E} = \pi/2$, the probabilities in Eq. (20) become sensitive to variations in ϕ_H, capturing the wave phenomenon in MZI_2.

After BS_3, the behavior becomes again corpuscular, following the same reasoning as after BS_1. Pessoa Júnior argued that these phase choices effectively represent each step of Afshar's setup. However, he also noted unresolved issues concerning the inclusion of the wire grid in the interferometric version. This motivated his proposal for the experiment explored in Sec. II D.

The standard MZI is well known for its instability in optical device applications. As a result, the Sagnac interferometer [61, 62] is often preferred in experimental settings due to its greater stability. However, to maintain the original structure of the experiments and ensure consistency with the original analysis of the complementarity relation, the simulation was performed on quantum computers using the formalism outlined in Sec. II A.

Since Afshar's experiment revolves around claims of violations of the BCP, the original approach is presented alongside demonstrative results from quantum computer simulations. Additionally, this analysis is revisited in Sec. II E in the context of the recently developed QCP proposed in Ref. [37], offering a fresh perspective on the interpretation of these experiments.

1. *Digital simulation of the modified Unruh's experiment*

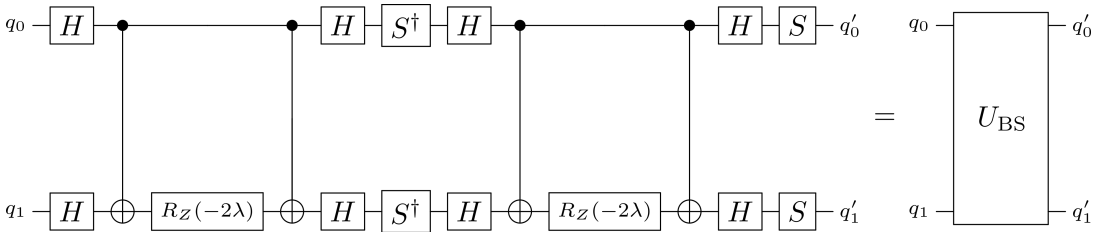

Figure 5: Quantum circuit for a BS, for which it is possible to control the transmission, T, and the reflection, R, coefficients ($\lambda = \frac{1}{2}\arctan\left(\frac{R}{T}\right)$). Each qubit represents one of the input modes. Following the execution of the circuit, the qubits that represent the input modes q_0, q_1 are converted into the output mode q_0', q_1'. For example, in Fig. 1 the input modes A (q_0) and B (q_1) are converted into the output modes C (q_0') and D (q_1'). The entire quantum circuit is represented by a box U_{BS}.

Following the formalism of Mohan *et al.* presented in Sec. II A, the digital simulation consists of mapping bosonic operators to Pauli operators and applying them to qubit states (representing the modes), which are mapped to Fock states. In the context of these experiments, the maximum occupation number of each mode is considered to be $n_j = 1\ \forall j$, and the total occupation number N is also equal to 1. To obtain the action of U_{BS} in states with this restriction, we first evolve the operators in the Heisenberg picture:

$$|1_{\mathrm{A}}, 0_{\mathrm{B}}\rangle = a^\dagger |0_{\mathrm{A}}, 0_{\mathrm{B}}\rangle = \left(Tc^\dagger + iRd^\dagger\right)|0_{\mathrm{C}}, 0_{\mathrm{D}}\rangle = T|1_{\mathrm{C}}, 0_{\mathrm{D}}\rangle + iR|0_{\mathrm{C}}, 1_{\mathrm{D}}\rangle\,, \tag{21}$$

$$|0_{\mathrm{A}}, 1_{\mathrm{B}}\rangle = b^\dagger |0_{\mathrm{A}}, 0_{\mathrm{B}}\rangle = \left(iRc^\dagger + Td^\dagger\right)|0_{\mathrm{C}}, 0_{\mathrm{D}}\rangle = iR|1_{\mathrm{C}}, 0_{\mathrm{D}}\rangle + T|0_{\mathrm{C}}, 1_{\mathrm{D}}\rangle\,. \tag{22}$$

The action of a balanced BS ($T = R = 1/\sqrt{2}$) on these states is then given (in the Schrödinger picture) by

$$|1_{\mathrm{A}}, 0_{\mathrm{B}}\rangle \xrightarrow{U_{\mathrm{BS}}} \frac{1}{\sqrt{2}}\left(|1_{\mathrm{C}}, 0_{\mathrm{D}}\rangle + i|0_{\mathrm{C}}, 1_{\mathrm{D}}\rangle\right), \tag{23}$$

$$|0_{\mathrm{A}}, 1_{\mathrm{B}}\rangle \xrightarrow{U_{\mathrm{BS}}} \frac{1}{\sqrt{2}}\left(i|1_{\mathrm{C}}, 0_{\mathrm{D}}\rangle + |0_{\mathrm{C}}, 1_{\mathrm{D}}\rangle\right), \tag{24}$$

which are well known superposition states for a single photon passing through a BS. The next step is mapping these states to qubit states. A general map between Fock and qubit states can be constructed as follows

$$|n_1, \cdots, n_m, \cdots\rangle_F \ \mapsto\ |n_1\rangle \otimes \cdots \otimes |n_m\rangle\,, \tag{25}$$

where the system was truncated at mode m for implementation purposes. Since the focus is on representing occupation numbers 0 and 1, and U_{BS} acts on a total of $m = 2$ modes, the map can be written as

$$|n_{\mathrm{A}},\ n_{\mathrm{B}}\rangle_F \ \mapsto\ |n_{\mathrm{A}}\rangle \otimes |n_{\mathrm{B}}\rangle\,, \tag{26}$$

with $n_{\mathrm{A}}, n_{\mathrm{B}} \in \{0, 1\} | n_{\mathrm{A}} + n_{\mathrm{B}} = 1$ and where the mode indices 1 and 2 were substituted by A and B, respectively. If the system were composed of $N \geq 2$ particles, codification methods (e.g. decimal to Gray code, discussed in Sec. II A) would be necessary to represent the numbers n_{A} and n_{B}; in our case, it is not necessary since 0 and 1 have the same representation in decimal, binary and Gray codes. Consequently, the map between the bosonic operators and Pauli operators in Eq. (13) is given by

$$a^\dagger|0_{\mathrm{A}}, 0_{\mathrm{B}}\rangle = |1_{\mathrm{A}}, 0_{\mathrm{B}}\rangle \mapsto (\mathcal{Q}_1 \otimes \mathbb{I})\,|0\rangle\,|0\rangle = |1\rangle\,|0\rangle\,, \tag{27}$$

$$a|1_{\mathrm{A}}, 0_{\mathrm{B}}\rangle = |0_{\mathrm{A}}, 0_{\mathrm{B}}\rangle \mapsto (\mathcal{Q}_0 \otimes \mathbb{I})\,|1\rangle\,|0\rangle = |0\rangle\,|0\rangle\,, \tag{28}$$

$$b^\dagger|0_{\mathrm{A}}, 0_{\mathrm{B}}\rangle = |0_{\mathrm{A}}, 1_{\mathrm{B}}\rangle \mapsto (\mathbb{I} \otimes \mathcal{Q}_1)\,|0\rangle\,|0\rangle = |0\rangle\,|1\rangle\,, \tag{29}$$

$$b|0_{\mathrm{A}}, 1_{\mathrm{B}}\rangle = |0_{\mathrm{A}}, 0_{\mathrm{B}}\rangle \mapsto (\mathbb{I} \otimes \mathcal{Q}_0)\,|0\rangle\,|1\rangle = |0\rangle\,|0\rangle\,. \tag{30}$$

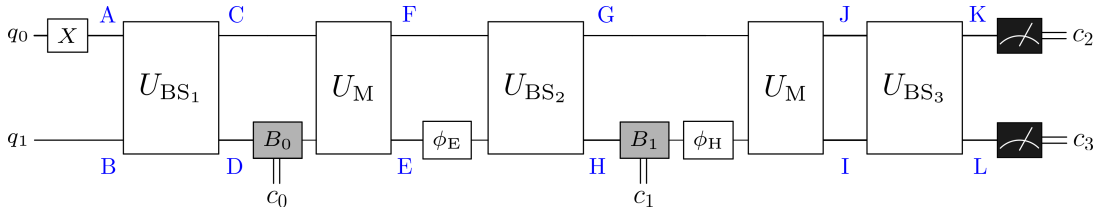

Figure 6: Quantum circuit for the modified Unruh's experiment. The state of qubits q_0 and q_1 correspond to the states of horizontal (A, C, F, G, J, K) and vertical (B, D, E, H, I, L) modes, respectively. The initial state prior to U_{BS_1} is $|\psi_0\rangle = |1\rangle_{\mathrm{A}}\,|0\rangle_{\mathrm{B}}$, with the X gate required to initiate mode A as occupied. The double lines denoted by c_0 and c_1 represent the classical bits storing the results registered by the blockers B_0 and B_1, respectively, and c_2 and c_3 by the detectors D_0 and D_1, respectively.

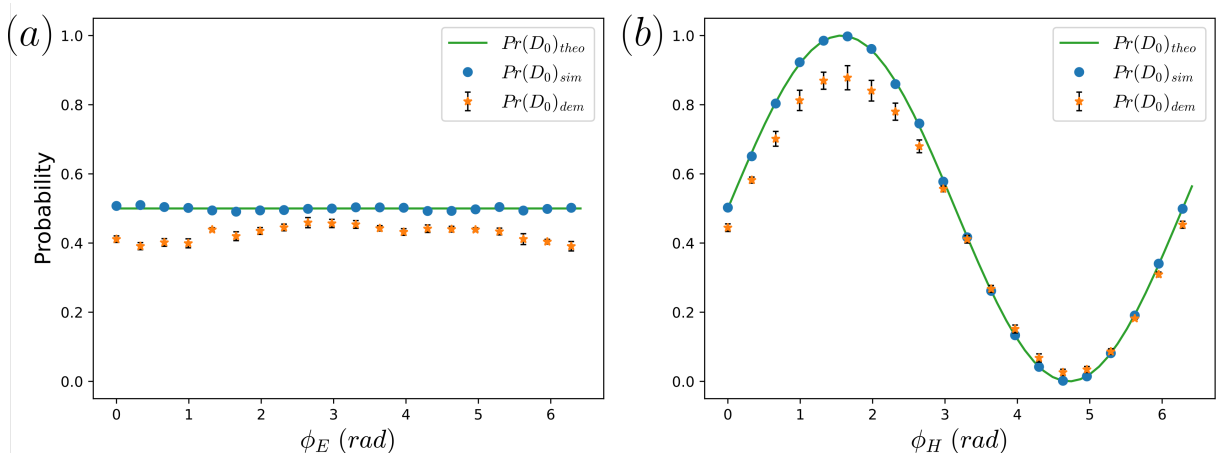

Figure 7: The graphs above illustrate the changes in probability at detector D_0 as a function of one of the phase shifts, while the other is fixed. (a) Probabilities for a variation of ϕ_{E}, with $\phi_{\mathrm{H}} = 0$ fixed. The interferometric visibility is theoretically zero, because the maximum and minimum probabilities are equal. This indicates a corpuscular behavior at MZI_1, as the phase variation does not produce changes in probability. (b) Probabilities for a variation of ϕ_{H}, with $\phi_{\mathrm{E}} = \pi/2$ fixed. This is interpreted as a wave-like behavior at MZI_2, as the phase variation now produces changes in probability, with $\max Pr(D_0) = 1$ and $\min Pr(D_0) = 0$. The error bars are the standard deviation for five repetitions of the demonstration using IBMQ and employed in the Eagle r3 processor ibm_sherbrooke quantum chip (its calibration parameters are given in Table II in Appendix E).

The map between the two-site bosonic interaction operators is thus

$$b^\dagger a + b a^\dagger \mapsto \frac{1}{2}(X \otimes X + Y \otimes Y), \tag{31}$$

and the unitary of the BS, presented in Eq. (1), is given by $U_{\mathrm{BS}} = e^{i\lambda(X\otimes X + Y\otimes Y)}$, where $\lambda = \theta/2$. Given that $[X \otimes X, Y \otimes Y] = \mathbb{0}$, it follows that

$$U_{\mathrm{BS}} = e^{i\lambda(X\otimes X)} e^{i\lambda(Y\otimes Y)}. \tag{32}$$

Figure 5 illustrates the quantum circuit for simulating a BS for any θ. In Appendix B, a complete derivation of the unitary form for a BS is provided, along with instructions on how to build the corresponding quantum circuit.

To simulate the modified Unruh's experiment in Fig. 4, let us first define the modes as: the input modes are set to q_0 (A) and q_1 (B) and are converted to the output modes q_0' (C) and q_1' (D). Next, it is necessary to reproduce the initial state denoted by $|\psi_0\rangle = |1_{\mathrm{A}}, 0_{\mathrm{B}}\rangle = |10\rangle_{\mathrm{AB}}$. As all qubits are initialized in the state $|0\rangle$ by default, one can apply the quantum gate X, represented by the unitary $X = |0\rangle\langle 1| + |1\rangle\langle 0|$, to qubit A to change into an occupied mode. To transform the quantum circuit in Fig. 5 into a quantum circuit for a BS represented in Fig. 5, it is necessary to set $\lambda = \pi/8$. Mirrors are also a particular case of the circuit in Fig. 5 by setting $\lambda = \pi/4$. In this case, modes C and D become F and E, respectively. The phase shifter is represented by the unitary $P(\phi_{\mathrm{mode}}) = |0\rangle\langle 0| + e^{i\phi_{\mathrm{mode}}}\,|1\rangle\langle 1|$, i.e., the term $e^{i\phi_{\mathrm{mode}}}$ is only applied if the mode is populated. After that, there is a repetition of the elements already mentioned with the appropriate adjustments in the modes: BS, $P(\phi_{\mathrm{H}})$, M and BS. Figure 6 shows the complete quantum circuit for the modified Unruh's experiment. The two parallel lines leading to the c's represent the storage of the classical bits registered by the blockers and the detectors D_0 and D_1.

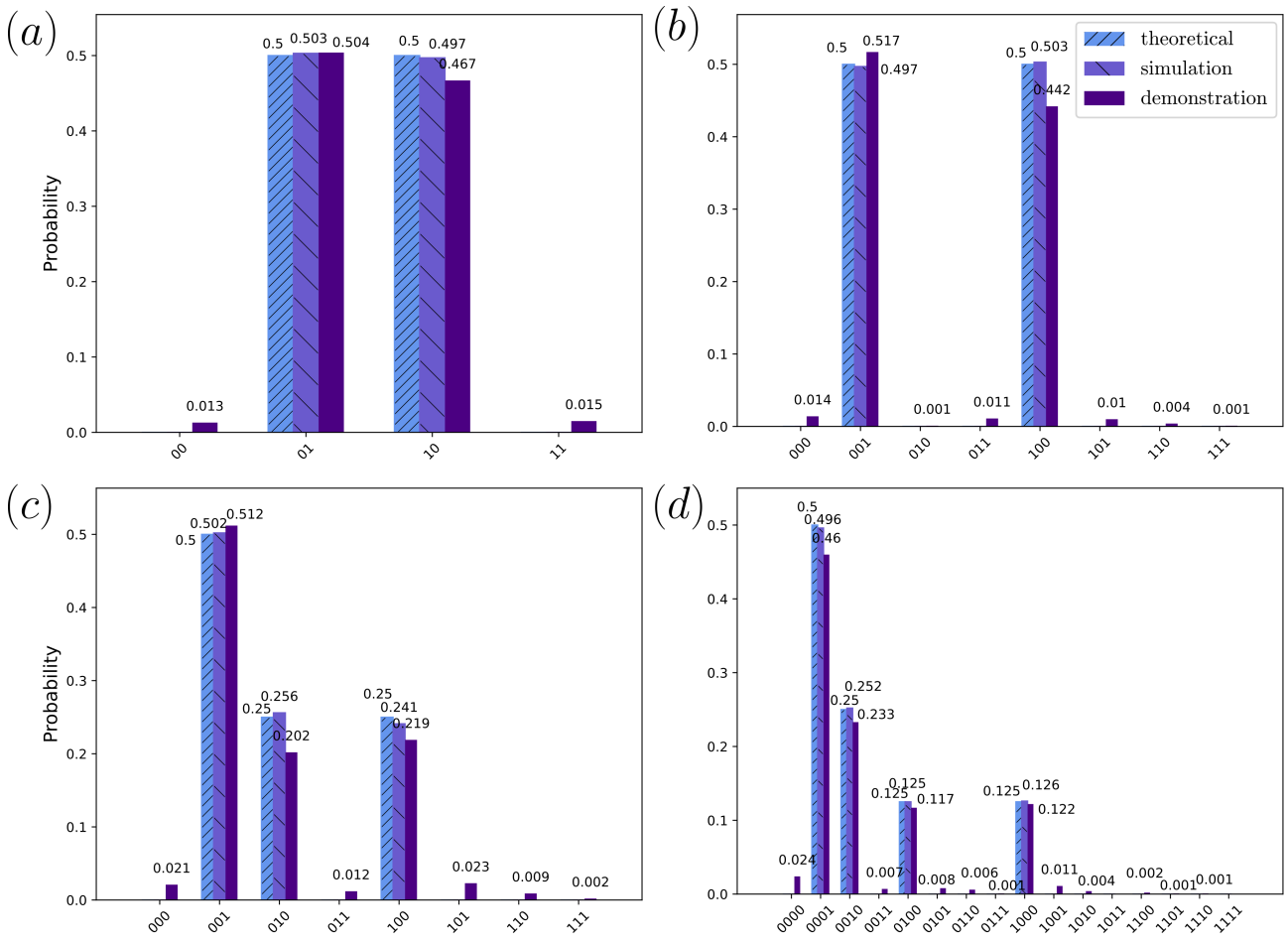

Figure 8: Histograms depicting the theoretical (bars with very close diagonal hatching), simulation (bars with widely spaced diagonal hatching), and demonstrations (solid bars) probabilities results for four different configurations of modified Unruh's experiment circuit: (a) no blocker inserted and the classical bits are composed by c_3c_2. The photons are detected either in D_0 (result 01) or D_1 (result 10); (b) blocker inserted in mode D and the classical bits are composed by $c_3c_2c_0$. About 50% of the photons hit the blocker B_0 (identified by the result 001) and the other 50% pass through the upper arm (mode C) and are detected in D_1 (identified by 100); (c) inserting only the blocker B_1 in mode H and the classical bits are composed by $c_3c_2c_1$. The H mode is no longer in vacuum state as in the original Unruh's experiment. About 50% of the photons hit the blocker B_1 (identified by the result 001) and the 25% is detected by each D_0 (identified by 010) and D_1 (identified by 100); and (d) both blockers inserted (modes D and H) and the classical bits are composed by $c_3c_2c_1c_0$. About half the photons hit the first blocker (0001), and of those which don't, about half (25%) hits the second blocker (0010). The photons that are not absorbed by either blockers are detected in both D_0 (0100) and D_1 (1000) which represents 12.5% in each detector. The demonstrative results are obtained utilizing IBMQ Eagle r3 processor ibm_kyiv quantum chip (its calibration parameters are given in Table III in Appendix E).

In the optical experiment, blockers absorb the photons and end the experiment, but in quantum computers there are no blockers to employ intrinsically. The solution is very simple in the mode notation and consists of a measuring device plus a resetting device to be able to perform the blocking simulation and measurements after BS_3 in a single setup. The resetting device converts any state to $|0\rangle$. Thus, a measurement device is inserted to get the result for that mode, and the resetting device turns the mode to the non-occupied state. If the mode is in the state $|0\rangle$, this means that there is no photon to block (vacuum state), the experiment continues and the reset device has no practical effect. In contrast, if the mode is in the state $|1\rangle$, the state should be set to $|0\rangle$, indicating that the photon was absorbed by the blocker. The experiment continues with a measurement after BS_3, analogous to when the photon is not blocked.

Figure 7 presents the graphs of probabilities for the conditions of phases $\phi_E = \pi/2$ and $\phi_H = 0$ considered by Pessoa Júnior. In Fig. 7 (a), the phase $\phi_H = 0$ is fixed while varying the ϕ_E. Theoretically, the visibility of Eq. (19) in the MZI_1 is zero, characterized by corpuscular behavior. In Fig. 7 (b), the phase $\phi_E = \pi/2$ is fixed while varying the ϕ_H. Theoretically, the visibility of Eq. (19) in the MZI_2 is one, characterized by wave behavior. In both

graphs, the solid green line represents the theoretical probability ($Pr(D_0)_{theo}$), the circular blue marks represent the classical simulation ($Pr(D_0)_{sim}$), and the orange star marks represent the demonstrative results ($Pr(D_0)_{dem}$) obtained using IBMQ quantum computers employed by the Eagle r3 processor ibm_sherbrooke quantum chip (its calibration parameters are given in Table II of the Appendix E). Despite the fact that the effects of noise and hardware constraints on quantum devices are well acknowledged and impact the final results, the demonstrative results are in reasonable agreement with theoretical predictions and classical simulations.

Before the analysis of the results in the histograms in Fig. 8, consider the following description: *i*) 8192 measurements are conducted for each demonstrative result, each producing a sequence of classical bits. *ii*) Fig. 6 indicates which measurement result is associated to which c_j, with $j = 0, 1, 2, 3$; c_0 is associated with the inclusions of blocker B_0, c_1 with blocker B_1, c_2 with detector D_0 and c_3 with detector D_1. *iii*) The binary numbers shown in the histogram are derived from measurements corresponding to a descending index of c_j within the quantum circuit illustrated in Fig. 6. *iv*) Every measurement procedure within the circuit yields an output: a result of 0 signifies a vacuum state (non-occupied mode), while a result of 1 indicates an occupied mode. In an ideal scenario, the measurement process will generate a series of bits proportional to the number of measurements performed, with only one bit being non-zero.

The histogram in Fig. 8 (*a*) shows the case without blockers, where the sequence 01 (10) $= c_3c_2$ means that about 50% of the photons are detected in D_0 (D_1). In Fig. 8 (*b*) the blocker B_0 is inserted in qubit q_1 (mode D); about 50% of the photons hit this blocker, producing the binary sequence $001 = c_3c_2c_0$. The sequence $100 = c_3c_2c_0$ means that about 50% of the detections occur in the detector D_1. According to Afshar, a detection in D_1 can be correlated to the upper path (mode C). Although the simulation with the blocker B_0 in mode C is not presented, the sequence 010 would correspond to a detection in D_0, which correlates to the lower path (mode D). Fig. 8 (c) shows the case where both paths are free and blocker B_1 is inserted in mode H. The binary number $001 = c_3c_2c_1$ means that about 50% of photons hit this blocker; the binary number $010 = c_3c_2c_1$ ($100 = c_3c_2c_1$) means that the photons that passed through were detected by the detector D_0 (D_1). This case differs from the original approach by Unruh, in the sense that mode H is not exclusively in the vacuum state anymore. Fig. 8 (*d*) shows the case with both blockers in place. About 50% of the photons hit blocker B_0 ($0001 = c_3c_2c_1c_0$), and about 25% hit the blocker B_1 ($0010 = c_3c_2c_1c_0$). The cases $0100 = c_3c_2c_1c_0$ and $1000 = c_3c_2c_1c_0$ represent the detection cases in D_0 and D_1, respectively. According to Pessoa Júnior, when modes C and D are free, the inclusion of B_1 is no longer possible since after the inclusion of B_0 the correlation between one path and one detector is no longer possible. In the following subsection, the experimental arrangement proposed by Pessoa Júnior is examined to demonstrate that the path-detector relation with the blocker B_1 in place still remains, similar to the presence of the wire grid in Afshar's experiment.

D. Pessoa Júnior's experiment - an enhancement of the modified Unruh's experiment

As shown in Sec. II C, Pessoa Júnior explores a modified version of Unruh's experiment to better capture the behavior of the quanton in each step of Afshar's experiment in Ref. [31] by adjusting phases in MZI_1 and MZI_2. However, when modes C and D are free, mode H, which was in the vacuum state in the version presented by Unruh, is no longer so. Moreover, the loss of photons by the insertion of the wire grid while each of the slits is blocked individually is not completely integrated into the modified Unruh's experiment. In view of this, Pessoa Júnior proposed another experimental apparatus as depicted in Fig. 9. The experimental setup consists of changing the mirrors in MZI_1 presented in Fig. 4 for BBSs (upper mirror for BBS_4 and lower mirror for BBS_5).

The discussion presented by Pessoa Júnior is deviated from at this point, and the experimental arrangement is adjusted to replicate certain aspects of Afshar's experiment. The same sequence as presented in Fig. 8 is followed and $\phi_H = \pi/2$ is included. The transmissibility for BBS's was set as $T_4^2 = T_5^2 = T^2 = 0.96$ to simulate the loss of photons when the slits are open and the wire grid is installed. The higher transmissibility can be understood as the region between the wire grid that allows the free flow of photons without blocking. The choice of T was made to obtain the 2% probability of quantons hitting the blocker B_1 which, in analogy to Afshar's experiment, is close to the amount of photons lost in this situation. With one arm blocked by B_0 and with B_1 in place, a fraction of probability reaches the detector D_1, around 0.5%, which simulates the photons arriving in the opposing detector expected and occasioned by the inclusion of the wire grid.

By incorporating BS_4 and BS_5 into the descriptions of the bosonic operators, two additional modes, E and F, appear in the vacuum state. The modes G and M (J and P), as well as the mode Q (R), lead to detector D_0 (D_1). Unlike the modified Unruh's experiment, detector D_0 (D_1) is related to the path C (D) and the adjustment is made in MZI_2 where the phase in mode N is set to $\phi_N = \pi$ to redirect the photons of modes C and D to the corresponding detector.

In the formal analysis, as before, the initial state is given by $|\psi_0\rangle = |1000\rangle_{ABEF}$ in which mode A is occupied by one photon. After BS_3, the state is given by $|\psi\rangle_{MQRP} = \frac{i}{\sqrt{2}}(|D_0\rangle + |D_1\rangle)$ where $|D_0\rangle = T|1000\rangle_{MQRP} - R|0100\rangle_{MQRP}$ and $|D_1\rangle = iT|0001\rangle_{MQRP} + R|0010\rangle_{MQRP}$ with $T_4 = T_5 = T$. The complete state evolution can be find in Appendix C.

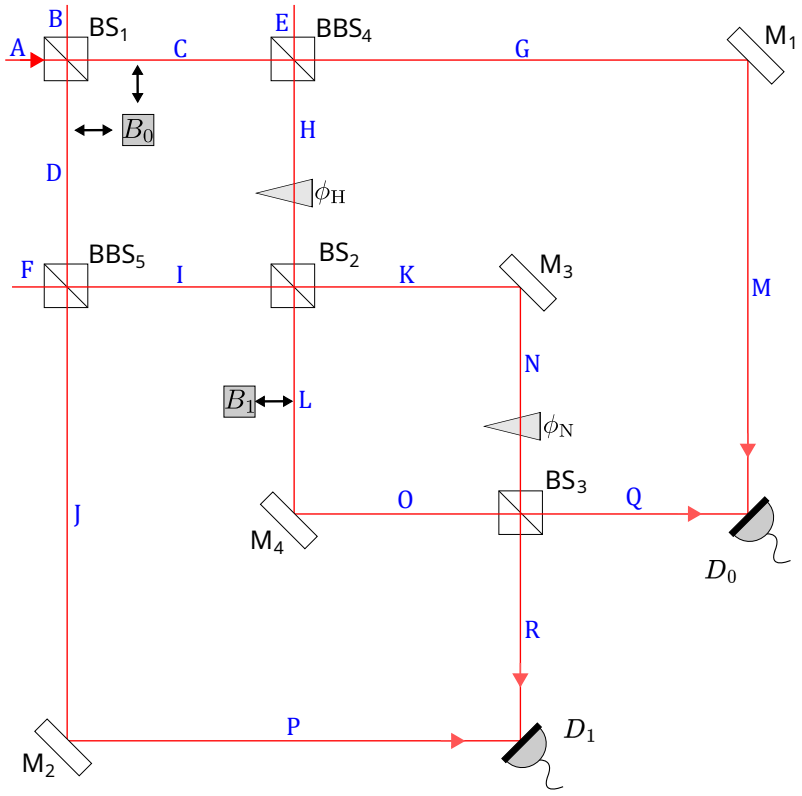

Figure 9: Pessoa Júnior's experiment is designed through examining the extra phase shifters incorporated into Unruh's model. In MZI_1 shown in Fig. 4, the mirrors were substituted by BBSs, namely BBS_4 and BBS_5 in the upper and lower arms of the interferometer, respectively. As discussed, Unruh's configuration blocks all the photons that pass through B_1, destroying the relationship between the path in MZI_1 and the detectors. The BBS's introduce two new modes, modes E and F, in the description of the quantum states. The transmissibility in BBS_4 and BBS_5 is adjusted to solve the problem introduced in Unruh's experiment after the inclusion of blocker B_1 and to align it with Afshar's experiment, where the relation between path and detector is made with the wire grid in place. The phase shift in mode H is set to $\phi_H = \pi/2$, as in the previous experimental setup; $\phi_N = \pi$ is used so that only one detector will trigger when blocking modes C or D.

In the absence of a blocker, the probability that a photon reaches detector D_0 or D_1 is 1/2.

Under the condition that blockers are present, the interaction-free measurement procedure introduced by Elitzur and Vaidman in Ref. [63] is employed in the description of the quantum states. The procedure for constructing states follows the same structure as described without blockers in Appendix C. The key is that the quantum state, which does not interact with the blocker, continues its unitary evolution as if it were a newly prepared state in the respective mode. With B_0 in place in mode D (the same approach can be used for B_0 in mode C), the state is given by $|\psi\rangle_{\mathrm{DMQR}} = \frac{i}{\sqrt{2}}(|B_0\rangle + |D_0\rangle)$, where $|B_0\rangle = |1000\rangle_{\mathrm{DMQR}}$ represents the quantum state of the photon just before interacting with the blocker B_0 and $|D_0\rangle = T\,|0100\rangle_{\mathrm{DMQR}} - R\,|0010\rangle_{\mathrm{DMQR}}$ represents the quantum state of the photon just before reaching the detector D_0. The probability of the photon being blocked or being detected by D_0 is 1/2. The path of the relation C and the detector D_0 is maintained following Afshar.

With B_1 in place, the state is given by $|\psi\rangle_{\mathrm{LMQRP}} = |B_1\rangle + |D_0\rangle + |D_1\rangle$ where $|B_1\rangle = \frac{iR}{2}(i-1)\,|10000\rangle_{\mathrm{LMQRP}}$, $|D_0\rangle = \frac{iT}{\sqrt{2}}\,|01000\rangle_{\mathrm{LMQRP}} - \frac{R(1-i)}{2\sqrt{2}}\,|00100\rangle_{\mathrm{LMQRP}}$, and $|D_1\rangle = -\frac{T}{\sqrt{2}}\,|00001\rangle_{\mathrm{LMQRP}} - \frac{R(1+i)}{2\sqrt{2}}\,|00010\rangle_{\mathrm{LMQRP}}$. Afshar *et al.* observed a photon loss of around 2% under conditions where both slits were simultaneously open and the wire grid was positioned in place. So, setting $T^2 = 0.96$, theoretically the probability that the quanton hits the blocker B_1 is around the probability of photon loss as reported by Afshar *et al.*. The probability of quantons being detected by D_0 or D_1 is 49%.

Finally, with B_0 in mode D and with B_1 in place, the state is given by $|\psi\rangle_{\mathrm{DLMQR}} = |B_0\rangle + |B_1\rangle + |D_0\rangle + |D_1\rangle$ where $|B_0\rangle = \frac{i}{\sqrt{2}}\,|10000\rangle_{\mathrm{DLMQR}}$, $|B_1\rangle = -\frac{R}{2}\,|010000\rangle_{\mathrm{DLMQR}}$, $|D_0\rangle = \frac{i}{\sqrt{2}}T\,|00100\rangle_{\mathrm{DLMQR}} - \frac{iR}{2\sqrt{2}}\,|00010\rangle_{\mathrm{DLMQR}}$, and $|D_1\rangle = -\frac{R}{2\sqrt{2}}\,|00001\rangle_{\mathrm{DLMQR}}$. The probability of the quanton being blocked by B_0 is 50%, 1% being blocked by B_1, 48.5% being detected by D_0 (the corresponding detector of mode C) and 0.5% being detected by the opposing detector D_1. The probability of being detected by the opposing detector is proportionally greater than that reported in

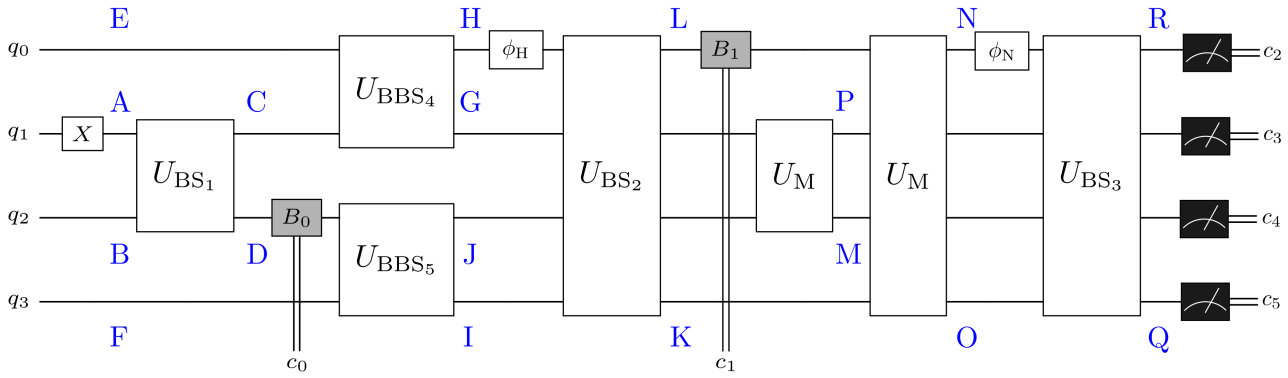

Figure 10: Quantum circuit for simulating the modified Pessoa Júnior's experiment. The state of qubits q_1 and q_3 (q_0 and q_2) correspond to the states of horizontal (vertical) modes, with the initial state before U_{BS_1} being $|\psi_0\rangle = |0\rangle_{\mathrm{E}}|1\rangle_{\mathrm{A}}|0\rangle_{\mathrm{B}}|0\rangle_{\mathrm{F}}$. In comparison to the previous setup, this version has two additional initial modes E and F which arise from the inclusion of U_{BBS_4} and U_{BS_5}. The double lines denoted by c_0 and c_1 represent the classical bits storing the results registered by the blockers. The results of measuring qubits q_0 and q_1 (q_2 and q_3) are stored in c_2 and c_3 (c_4 and c_5), which correspond to the detections made by detector D_1 (D_0) as depicted in Fig. 9.

Afshar's experiment, but highlights that the inclusion of the blocker B_1 affects the path-detector relation. Otherwise, this experimental setup fails to simulate the great loss of photon count caused by the presence of the wire grid, which is reported to be approximately 14% in the original experiment.

1. *Digital simulation of Pessoa Júnior's experiment*

The digital simulation of the experimental version proposed by Pessoa Júnior follows the same idea as that constructed in Sec. II C 1 and the Eqs. (30)-(32) are the same. The major difference is that there is the exchange of MZI_1 mirrors for BBSs. There are two new input modes (E and F, both in the vacuum state) represented by the qubits q_0 and q_3 in Fig. 10. The initial state with inputs in modes A and B in Fig. 9 is now initialized in the qubits q_1 and q_2, respectively. As before, the initial state is $|\psi_0\rangle = |1000\rangle_{\mathrm{ABEF}}$, which is produced applying the Pauli X gate in qubit q_1 and with the inclusion of the modes added by the BBSs, E and F. Then the initial state passes through U_{BS_1} and the output C (D) enters a BBS with mode E (F). The output H (q_0), after applying the phase shifter $\phi_{\mathrm{H}} = \pi/2$, and I ($q_3$) enter another BS ($\mathrm{BS}_2$ in Fig. 9), then mirrors, $\phi_{\mathrm{N}} = \pi$ and then $q_0 = \mathrm{N}$ and $q_1 = \mathrm{O}$ pass through U_{BS_3}. There are mirrors that change the modes G and J to M and P, respectively. Subsequently, the detector D_0 (D_1) registers a click, as demonstrated in Fig. 9, which depicts the detection process. Quantons from the M and Q modes are detected by D_1, whereas those originating from the P and R modes are detected by D_0. The measurement results are encoded in classical bits: c_0 is assigned to the blocker B_0, and c_1 is linked to the blocker B_1. Detections at D_1 are noted as the addition $c_2 + c_3$, while D_0 detections are recorded as $c_4 + c_5$.

In Fig. 11 (a) is the scenario when none of the blockers are inserted and the result is composed of the classical bits $c_5c_4c_3c_2$. The detection in D_0 is $c_2 + c_3 = 0001 + 0010$ and in D_1 is $c_4 + c_5 = 0100 + 1000$, which corresponds to around 50% in each detector. Fig. 11 (b) is the case where B_0 is inserted and the result is constructed by $c_5c_4c_3c_2c_0$; the probability of a quanton being blocked by B_0 is about 50%. The results $01000 + 10000$ correspond to the detection in D_0. Fig. 11 (c) is the scenario in which B_1 is inserted and the classical bits are formed by $c_5c_4c_3c_2c_1$. The result 00001 corresponds to quantons blocked by B_1, which is the case where Afshar *et al.* perceive a reduction in photon count by the insertion of the wire grid. The composed result of the clicks in $01000 + 10000$ ($00100 + 00010$) is the detector D_0 (D_1). This case is constructed to correspond to the amount of 2% quantons blocking by B_1. Fig. 11 (d) shows the case with both blockers in place, where the results correspond to $c_5c_4c_3c_2c_1c_0$. The blocker B_0 reduces the final count in 50% followed by a reduction of 1% in the blocker B_1. The composed result of the clicks in $01000 + 10000$ (48.5%) correspond to detector D_0 and $00100 + 00010$ (0.5%) correspond to detector D_1. The classical simulation closely adheres to the theoretical framework. However, similar to the modified Unruh's experiment, the demonstrative results are influenced by noise and environmental interactions within quantum computers. The demonstrative results reveal numerous instances where the photon count per mode is not preserved. To improve visual clarity, the histogram excludes part of the demonstrative results that fit this condition. The complete results are provided in Table I in Appendix D.

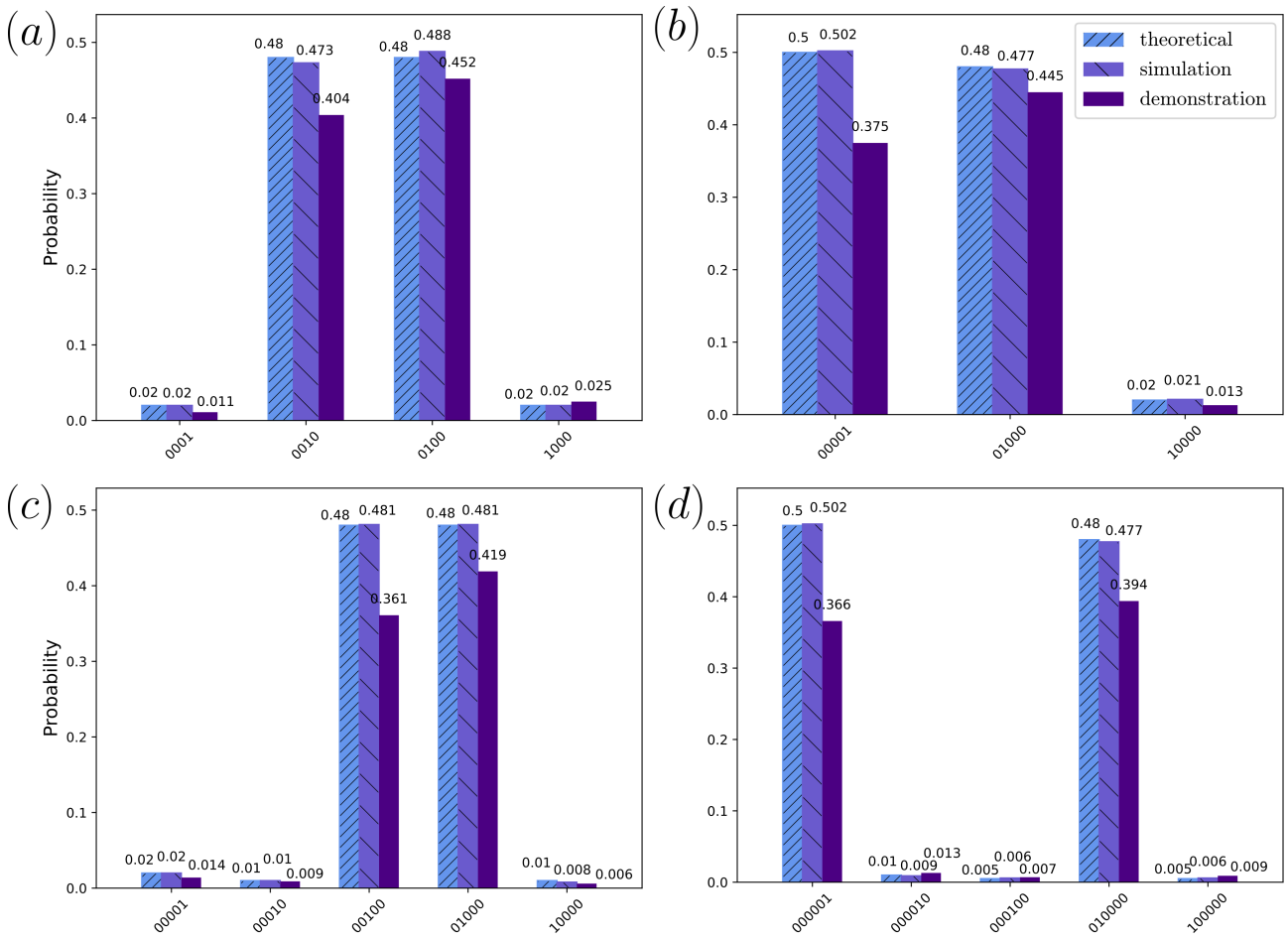

Figure 11: Histograms depicting the theoretical (bars with very close diagonal hatching), simulation (bars with widely spaced diagonal hatching), and demonstrations (solid bars) probability results for four different configurations of Pessoa Júnior's experiment circuit: (*a*) no blocker inserted and classical bits composed by $c_5c_4c_3c_2$. Detections in D_1 correspond to the sum of results 0001 and 0010, and detections in D_0 to the sum of results 0100 and 1000; (*b*) blocker B_0 inserted in mode D and classical bits composed by $c_5c_4c_3c_2c_0$. About 50% of photons hit the blocker (identified by the result 00001) and the other 50% pass through the upper arm (mode C) and are detected in D_0 (identified by the sum of results 01000 and 10000; (*c*) blocker B_1 inserted in mode L and classical bits composed by $c_5c_4c_3c_2c_1$. The 2% of quantons that hit blocker B_1 represent the photons that hit the wire grid in Afshar's experiment with both slits open. Detections in D_0 correspond to the sum of results 10000 and 01000, and detections in D_1 to the sum of results 00010 and 00100; and (*d*) both blockers inserted and classical bits composed by $c_5c_4c_3c_2c_1c_0$. The photons that are not blocked by B_0 (000001) nor B_1 (000010) are detected in both D_1 (000100) and D_0 (sum of 010000 and 100000). To improve visual clarity, the histograms don't include part of the demonstrative results which do not preserve the photon count per mode. The complete results are provided in Table I of Appendix D. The demonstrative results are obtained utilizing IBMQ Eagle r3 processor ibm_kyiv quantum chip (its calibration parameters are given in Table III in Appendix E.)

E. Discussion and analysis of the experiments in the light of the quantum complementarity principle

Interferometric experiments of this type generally aim to characterize the dual nature of the quanton after its interaction with the first BS by employing complementarity relations constructed in an *ad hoc* manner for the entire experimental setup. Significant efforts have been made to modify these setups and develop alternative approaches for constructing complementarity relations. However, despite these variations, the fundamental objective remains the same as in the MZI depicted in Fig. 2: determining the quanton's behavior after the first BS.

A key distinction in the modified version of Unruh's experiment lies in the functions used to quantify the particle-like (P) and wave-like (W) behaviors. It is important to note that many complementarity relations – particularly those relying on interferometric visibility to quantify W – invoke retroactive inference, as the quantification does not occur in the region where the wave-like behavior is manifested. Afshar, however, shifts this perspective by using retroactive

inference to quantify P, while W is inferred non-destructively via the wire grid precisely where the phenomenon manifests.

Pessoa Júnior, in his analysis, argued that Afshar's experiment does not violate the complementarity relation. Instead, by shifting the viewpoint from Bohr's interpretation of the experiment as a whole to an analysis at each stage of the process, he concluded that complementarity remains valid at every step. This perspective aligns closely with the QCP, which is derived directly from the postulates of QM. The validity of this interpretation will be further explored below using the QCRs in the MZI setup shown in Fig. 2.

Let us derive the QCR for the standard MZI experiment, as depicted in Fig. 2. Consider an initial state $|10\rangle_{\mathrm{AB}}$. After passing through the first biased beam splitter (BBS_1), the state evolves into

$$|\psi_1\rangle = T_1 |10\rangle_{\mathrm{AB}} + iR_1 |01\rangle_{\mathrm{AB}} . \tag{33}$$

For this pure-state scenario, the QCR from Eq. (17) simplifies to

$$C_{l_1}(\rho_t) + P_{l_1}(\rho_t) = 1. \tag{34}$$

From the perspective of the QCP, any state within the MZI – whether immediately after BBS_1, after the mirrors, or following the phase shifter – yields the same QCR result. For simplicity, we consider the state $|\psi_1\rangle$. Since its corresponding density matrix is $\rho_1 = |\psi_1\rangle\langle\psi_1|$, the QCR provides the following wave-like ($\mathfrak{W}$) and particle-like ($\mathfrak{P}$) quantifications:

$$\mathfrak{W}(\rho_1) = C_{l_1}(\rho_1) = 2T_1R_1, \tag{35}$$
$$\mathfrak{P}(\rho_1) = P_{l_1}(\rho_1) = 1 - 2T_1R_1. \tag{36}$$

According to the QCR, the interplay between wave-like and particle-like properties remains complementary at each instant, as captured by the state ρ. Notably, in this scenario, these behaviors are governed solely by the transmission (T) and reflection (R) coefficients of the first biased beam splitter. When T and R are balanced, the state after BBS_1 exhibits maximal wave-like behavior, manifesting as a superposition. As T deviates from balance – either increasing or decreasing – predictability ($\mathfrak{P}$) grows, akin to a betting game where the probability of determining the quanton's path increases.

The explanation of the experiment in Fig. 2 using the QCP also extends to the modified Unruh's experiment (Fig. 4) and Pessoa Júnior's experiment (Fig. 9). This follows from the fact that BBS_1 in these setups is a generalization of BS_1, which corresponds to the specific case where $T_1 = R_1 = 1/\sqrt{2}$. Since all these experimental configurations are designed to analyze the quanton's dual behavior after the first beam splitter, their description follows naturally from the QCP framework.

Although Pessoa Júnior provides an insightful perspective by analyzing each stage of Afshar's experiment and its interferometric variants individually – concluding that no single step violates the BCP – he still considers a retroactive influence on the quanton's dual behavior. Specifically, in the modified Unruh experiment, he argues that adjusting the phase ϕ_{E} of MZI_2 affects the behavior within MZI_1.

From the perspective of the QCP, while the quantification at each step via ρ_t aligns with Pessoa Júnior's approach, the notion of retrocausal influence is not supported. In the modified Unruh experiment, the quanton's behavior immediately after BS_1 is always wave-like, and modifying ϕ_{H} does not alter its behavior within MZI_1. However, after BS_2, the quanton's behavior does become dependent on the choice of ϕ_{H}, as this phase determines the state within MZI_2, allowing for a full spectrum from maximal wave-like behavior ($\mathfrak{W}$) to maximal particle-like behavior ($\mathfrak{P}$). Similarly, modifying ϕ_{E} does not affect behavior within MZI_2.

A comparable situation occurs after BS_3, where the values of $\mathfrak{W}$ and $\mathfrak{P}$ depend on the state prepared before entering BS_3. Ultimately, this state is determined by the choices of ϕ_{E} and ϕ_{H}, but not in a retroactive manner. A related discussion on causality in quantum experiments was explored in Ref. [37], particularly in the context of Wheeler 's delayed-choice experiment (WDCE). It is worth mentioning that in Ref. [64] a classical causal model was constructed for WDCE.

III. FINAL REMARKS

In this work, we explored the digital quantum simulation of interferometric alternatives to Afshar's experiment. Using the formalism recently introduced by Mohan *et al.*, which maps bosonic operators to Pauli operators, we simulated two versions of nested MZIs proposed by Pessoa Júnior. While the modified Unruh experiment requires

only a single qubit for implementation on a quantum computer, the version proposed by Pessoa Júnior involves significantly more complex quantum circuits, making the simulation particularly innovative.

Our results align well with theoretical predictions for both experiments. Unlike the Hong-Ou-Mandel simulation discussed by Mohan *et al.*, our simulations were simplified by avoiding trotterization techniques. This was possible because the unitary matrix corresponding to the BS can be expressed as a product of exponentials, leveraging the commutativity of operators, such as $[X\otimes X, Y\otimes Y] = \mathbb{O}$. Consequently, each exponential could be directly decomposed into basic quantum gates, enabling efficient implementation on quantum computers.

By providing a digital quantum simulation of the nested MZI, this work also examines the issues raised by Afshar regarding a potential violation of BCP. Afshar's approach, which relies on non-destructive measurements to quantify the wave behavior of the quanton, combined with the lack of a formal definition of the BCP, allowed for the construction of an *ad hoc* complementarity relation that seemingly violates the BCP.

Our digital quantum simulation offers both a classical simulation and demonstrative results on quantum computers, which show strong agreement with theoretical predictions. Pessoa Júnior's analysis of the modified Unruh experiment incorporates a phase into each MZI, concluding that each stage of the experiment corresponds to specific behaviors analogous to those observed in Afshar's original experiment. Inspired by these findings, Pessoa Júnior proposed a new experimental setup to simulate additional aspects of Afshar's experiment.

Our simulations reveal that the observed 2% reduction in photon count caused by the wire grid can be replicated when both paths are unobstructed and with B_1 in place. Furthermore, the inclusion of the blocker B_0 in mode D, alongside B_1, successfully simulates detection at the opposing detector, consistent with the experimental results of Afshar. However, it should be noted that this version of the interferometric setup cannot fully replicate all the nuances explored in the original experiment.

Finally, the QCP, along with its key elements for evaluating wave-particle duality through Quantitative Complementarity Relations (QCRs), was discussed. Pessoa Júnior argued in his work that Afshar's experiment and its interferometric variations do not violate the quantitative version of BCP. He maintained that wave-particle duality holds true at each stage of the experimental apparatus, even though his analysis relies on retroactive inference, a standard approach in the literature for addressing wave-particle duality.

A critical aspect of the QCP, in agreement with Pessoa Júnior's interpretation, involves quantifying QCRs at each experimental step without invoking retrocausality. The wave-like ($\mathfrak{W}$) and particle-like ($\mathfrak{P}$) behaviors are quantified through the unitary evolution of the system's quantum state, ρ_t, precisely where the phenomena manifest. This method ensures the internal consistency of the complementarity between $\mathfrak{W}$ and $\mathfrak{P}$ within the QCR framework.

By revisiting how the QCP resolves paradoxes, such as those posed by Afshar's experiment, this work also demonstrates that quantum computers are highly adaptable and effective platforms for simulating experiments involving bosonic systems. . These findings further reinforce the utility of digital quantum simulations in configurations that deviate from the conventional, such as the one shown in Fig. 9, to further expand the exploration of QM fundamentals.

Acknowledgments

This work was supported by the Coordination for the Improvement of Higher Education Personnel (CAPES) under Grant No. 88887.827989/2023-00, by the Research Support Foundation of the State of Rio Grande do Sul (FAPERGS) under Grant No. 23/2551-0001199-9, by the National Council for Scientific and Technological Development (CNPq) under Grants No. 309862/2021-3, No. 409673/2022-6, and No. 421792/2022-1, and by the National Institute for the Science and Technology of Quantum Information (INCT-IQ) under Grant No. 465469/2014-0.

Appendix A: Relations between input and output bosonic operators for arbitrary θ

For illustration, let us examine the relationship between input modes A and B and output mode C. In this case, we have

$$c = U_{DF}^{\dagger}\, a\, U_{DF} = \left(e^{i\theta(b^{\dagger}a+ba^{\dagger})}\right)^{\dagger} a\; e^{i\theta(b^{\dagger}a+ba^{\dagger})} = e^{-i\theta(ab^{\dagger}+a^{\dagger}b)} a\; e^{i\theta(b^{\dagger}a+ba^{\dagger})} = e^{-i\theta(b^{\dagger}a+ba^{\dagger})} a\; e^{i\theta(b^{\dagger}a+ba^{\dagger})}, \tag{A1}$$

since $\left[a, b^{\dagger}\right] = 0$ and $\left[a^{\dagger}, b\right] = 0$. Using the Baker−Hausdorff lemma,

$$e^{\gamma H} a\; e^{-\gamma H} = a + \gamma\left[H, a\right] + \frac{\gamma^2}{2!}\left[H, \left[H, a\right]\right] + \frac{\gamma^3}{3!}\left[H, \left[H, \left[H, a\right]\right]\right] + \cdots, \tag{A2}$$

with $\gamma = -i\theta$ and $H = b^\dagger a + b a^\dagger$, it follows that

$$c = a - i\theta \left[b^\dagger a + b a^\dagger, a\right] - \frac{\theta^2}{2!}\left[b^\dagger a + b a^\dagger, \left[b^\dagger a + b a^\dagger, a\right]\right] + \cdots . \tag{A3}$$

Given that

$$\left[b^\dagger a + b a^\dagger, a\right] = \left[b^\dagger a, a\right] + \left[b a^\dagger, a\right] = b^\dagger \left[a, a\right] + \left[b^\dagger, a\right] a + b \left[a^\dagger, a\right] + \left[b, a\right] a^\dagger = -b \left[a, a^\dagger\right] = -b, \tag{A4}$$

and

$$\begin{aligned}\left[b^\dagger a + b a^\dagger, \left[b^\dagger a + b a^\dagger, a\right]\right] &= \left[b^\dagger a + b a^\dagger, -b\right] = -\left(\left[b^\dagger a, b\right] + \left[b a^\dagger, b\right]\right) \\ &= -\left(b^\dagger \left[a, b\right] + \left[b^\dagger, b\right] a + b \left[a^\dagger, b\right] + \left[b, b\right] a^\dagger\right) = -\left(-\left[b, b^\dagger\right] a\right) = a,\end{aligned} \tag{A5}$$

one obtains

$$\begin{aligned}c &= a + i\theta b - \frac{\theta^2}{2!}a - i\frac{\theta^3}{3!}b + \frac{\theta^4}{4!}a + i\frac{\theta^5}{5!}b + \cdots = a\left(1 - \frac{\theta^2}{2!} + \frac{\theta^4}{4!} + \cdots\right) + ib\left(\theta - \frac{\theta^3}{3!} + \frac{\theta^5}{5!} + \cdots\right) \\ &= a\cos(\theta) + ib\sin(\theta),\end{aligned} \tag{A6}$$

and thus

$$c^\dagger = a^\dagger \cos(\theta) - ib^\dagger \sin(\theta). \tag{A7}$$

Similarly, this holds for the relationship between input modes A and B and the output mode D:

$$\begin{aligned}d &= ia\sin(\theta) + b\cos(\theta), \\ d^\dagger &= -ia^\dagger \sin(\theta) + b^\dagger \cos(\theta).\end{aligned} \tag{A8}$$

Defining $T = \cos\theta$ and $R = \sin\theta$, Eqs. (2) through Eqs. (3) are derivable.

Appendix B: Beam splitter unitary implementation

In order to implement the unitary transformation of the BS, it is initially useful to implement the unitary $U = \exp\left[i\lambda\left(Z \otimes Z\right)\right]$. The spectral decomposition of $Z \otimes Z$ is given by

$$Z \otimes Z = \left(|0\rangle\langle 0| - |1\rangle\langle 1|\right) \otimes \left(|0\rangle\langle 0| - |1\rangle\langle 1|\right) = \left(|00\rangle\langle 00| + |11\rangle\langle 11|\right) - \left(|01\rangle\langle 01| + |10\rangle\langle 10|\right), \tag{B1}$$

and consequently, the spectral decomposition of U reads

$$\exp\left[i\lambda\left(Z \otimes Z\right)\right] = e^{i\lambda}\left(|00\rangle\langle 00| + |11\rangle\langle 11|\right) + e^{-i\lambda}\left(|01\rangle\langle 01| + |10\rangle\langle 10|\right). \tag{B2}$$

Noting that

$$C_X^{0\to 1}\left(\mathbb{I} \otimes e^{i\lambda Z}\right) C_X^{0\to 1} = e^{i\lambda}\left(|00\rangle\langle 00| + |11\rangle\langle 11|\right) + e^{-i\lambda}\left(|01\rangle\langle 01| + |10\rangle\langle 10|\right) = \exp\left[i\lambda\left(Z \otimes Z\right)\right] \tag{B3}$$

and that

$$e^{i\lambda Z} = e^{i\lambda}|0\rangle\langle 0| + e^{-i\lambda}|1\rangle\langle 1| = e^{i\lambda}\begin{bmatrix}1 & 0\\ 0 & 0\end{bmatrix} + e^{-i\lambda}\begin{bmatrix}0 & 0\\ 0 & 1\end{bmatrix} = \begin{bmatrix}e^{i\lambda} & 0\\ 0 & e^{-i\lambda}\end{bmatrix} = R_Z(-2\lambda), \tag{B4}$$

the unitary U can be written as

$$\exp\left[i\lambda\left(Z \otimes Z\right)\right] = C_X^{0\to 1}\left[\mathbb{I} \otimes R_Z(-2\lambda)\right] C_X^{0\to 1}, \tag{B5}$$

which is implemented in a quantum circuit as shown in Fig. 12 (a).

To implement the terms of U_{BS}, we begin by writing their spectral decomposition as

$$\exp\left[i\lambda(X \otimes X)\right] = e^{i\lambda}\left(|{+}{+}\rangle\langle{+}{+}| + |{-}{-}\rangle\langle{-}{-}|\right) + e^{-i\lambda}\left(|{+}{-}\rangle\langle{+}{-}| + |{-}{+}\rangle\langle{-}{+}|\right) \tag{B6}$$

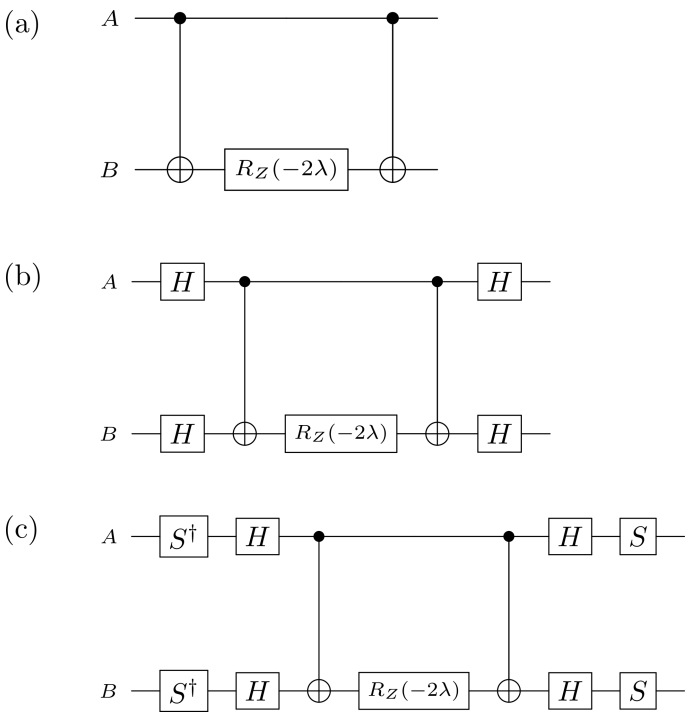

Figure 12: Quantum circuits that implement the unitary transformations (a) $e^{i\lambda(Z\otimes Z)}$, (b) $e^{i\lambda(X\otimes X)}$ and (c) $e^{i\lambda(Y\otimes Y)}$.

and

$$\exp\left[i\lambda(Y\otimes Y)\right] = e^{i\lambda}\big(\,|\oplus\oplus\rangle\langle\oplus\oplus| + |\ominus\ominus\rangle\langle\ominus\ominus|\,\big) + e^{-i\lambda}\big(\,|\oplus\ominus\rangle\langle\oplus\ominus| + |\ominus\oplus\rangle\langle\ominus\oplus|\,\big), \tag{B7}$$

where $|\pm\rangle = (|0\rangle \pm |1\rangle)/\sqrt{2}$, $|\oplus\rangle = (|0\rangle + i|1\rangle)/\sqrt{2}$, and $|\ominus\rangle = (|0\rangle + i|1\rangle)/\sqrt{2}$. Since the Hadamard gate H switches between the computational basis and the X basis, one can write

$$\exp\left[i\lambda(X\otimes X)\right] = H\otimes H\left[e^{i\lambda}(|00\rangle\langle 00| + |11\rangle\langle 11|) + e^{-i\lambda}\big(\,|01\rangle\langle 01| + |10\rangle\langle 10|\,\big)\right] H\otimes H. \tag{B8}$$

The term in brakets corresponds to the spectral decomposition of $\exp\left[i\lambda\big(Z\otimes Z\big)\right]$, so that

$$\exp\left[i\lambda\big(X\otimes X\big)\right] = H\otimes H\big(C_X^{0\to 1}\big)\mathbb{I}\otimes R_Z(-2\lambda)\big(C_X^{0\to 1}\big)H\otimes H, \tag{B9}$$

and analogously for the other term

$$\exp\left[i\lambda\big(Y\otimes Y\big)\right] = S\otimes S\exp\left[i\lambda\big(X\otimes X\big)\right]S^\dagger\otimes S^\dagger. \tag{B10}$$

Figure 12 (b) illustrates the quantum circuit corresponding to $e^{i\lambda(X\otimes X)}$, while Fig. 12 (c) depicts the circuit for $e^{i\lambda(Y\otimes Y)}$.

Appendix C: Formal analysis of Pessoa Júnior's experiment

As before, an initial state in which mode A is populated by one photon is considered, $|\psi_0\rangle = |1_\mathrm{A}, 0_\mathrm{B}, 0_\mathrm{E}, 0_\mathrm{F}\rangle$. After BS_1 the state is evolved to

$$|\psi_1\rangle = \frac{1}{\sqrt{2}}\big(\,|1_\mathrm{C}, 0_\mathrm{E}, 0_\mathrm{D}, 0_\mathrm{F}\rangle + i\,|0_\mathrm{C}, 0_\mathrm{E}, 1_\mathrm{D}, 0_\mathrm{F}\rangle\,\big); \tag{C1}$$

even though modes E and F are included for completeness, they remain non populated. In the following, we present the most general states for the remaining optical elements. After BS_4 and BS_5 we have

$$|\psi_2\rangle = \frac{1}{2}\big(T_4\,|1_{\rm G},0_{\rm H},0_{\rm I},0_{\rm J}\rangle + iR_4\,|0_{\rm G},1_{\rm H},0_{\rm I},0_{\rm J}\rangle - R_5\,|0_{\rm G},0_{\rm H},1_{\rm I},0_{\rm J}\rangle + iT_5\,|0_{\rm G},0_{\rm H},0_{\rm I},1_{\rm J}\rangle\big), \tag{C2}$$

where the coefficients T_4 and R_4 (T_5 and R_5) correspond to the ability to adjust the transmission and reflection in $\rm BS_4$ ($\rm BS_5$) and $T_j^2 + R_j^2 = 1$ with $T_j, R_j \in \mathbb{R}$ for $j = 4, 5$.

After $\phi_{\rm H}$, the quantum state is

$$|\psi_3\rangle = \frac{1}{2}\big(T_4\,|1_{\rm G},0_{\rm H},0_{\rm I},0_{\rm J}\rangle + iR_4e^{i\phi_H}\,|0_{\rm G},1_{\rm H},0_{\rm I},0_{\rm J}\rangle - R_5\,|0_{\rm G},0_{\rm H},1_{\rm I},0_{\rm J}\rangle + iT_5\,|0_{\rm G},0_{\rm H},0_{\rm I},1_{\rm J}\rangle\big). \tag{C3}$$

After $\rm BS_2$, we obtain the following state:

$$\begin{aligned}|\psi_4\rangle = \frac{1}{2}\big(T_4\,|1_{\rm G},0_{\rm K},0_{\rm L},0_{\rm J}\rangle + iT_5\,|0_{\rm G},0_{\rm K},0_{\rm L},1_{\rm J}\rangle\big) - \frac{1}{2\sqrt{2}}\big(R_5 + R_4e^{i\phi_H}\big)\,|0_{\rm G},1_{\rm K},0_{\rm L},0_{\rm J}\rangle \\ - \frac{i}{2\sqrt{2}}\big(R_5 - R_4e^{i\phi_H}\big)\,|0_{\rm G},0_{\rm K},1_{\rm L},0_{\rm J}\rangle\,.\end{aligned} \tag{C4}$$

The action of mirrors and $\phi_{\rm N} = \pi$ leads to

$$\begin{aligned}|\psi_5\rangle = \frac{i}{2}\big(T_4\,|1_{\rm M},0_{\rm N},0_{\rm O},0_{\rm P}\rangle + iT_5\,|0_{\rm M},0_{\rm N},0_{\rm O},1_{\rm P}\rangle\big) + \frac{i}{2\sqrt{2}}\big(R_5 + R_4e^{i\phi_H}\big)\,|0_{\rm M},1_{\rm N},0_{\rm O},0_{\rm P}\rangle \\ + \frac{1}{2\sqrt{2}}\big(R_5 - R_4e^{i\phi_H}\big)\,|0_{\rm M},0_{\rm N},1_{\rm O},0_{\rm P}\rangle\,.\end{aligned} \tag{C5}$$

After $\rm BS_3$, we get

$$\begin{aligned}|\psi_6\rangle = \frac{i}{2}\big(T_4\,|1_{\rm M},0_{\rm Q},0_{\rm R},0_{\rm P}\rangle + iT_5\,|0_{\rm M},0_{\rm Q},0_{\rm R},1_{\rm P}\rangle\big) \\ + \frac{1}{4}\Big[-\big(R_5 + R_4e^{i\phi_H}\big) + e^{i\phi_L}\big(R_5 - R_4e^{i\phi_H}\big)\Big]\,|0_{\rm M},1_{\rm Q},0_{\rm R},0_{\rm P}\rangle \\ - \frac{i}{4}\Big[-\big(R_5 + R_4e^{i\phi_H}\big) - e^{i\phi_L}\big(R_5 - R_4e^{i\phi_H}\big)\Big]\,|0_{\rm M},0_{\rm Q},1_{\rm R},0_{\rm P}\rangle\,.\end{aligned} \tag{C6}$$

Appendix D: Complete demonstrative results for Figure 11

The complete results for the demonstrations of Figure 11, including those appearing due to hardware noise, are shown in Table I.

Table I: Probabilities of each outcome in the implementation of Pessoa Júnior's circuit in a quantum hardware. This table includes less significant outcomes that are not shown in the histograms of Figure 11.

Figure 11(a)		Figure 11(b)		Figure 11(c)		Figure 11(d)	
Result	Probability	Result	Probability	Result	Probability	Result	Probability
0000	0.0287	00000	0.0269	00000	0.0287	000000	0.0219
0001	0.0115	00001	0.3745	00001	0.0139	000001	0.3657
0010	0.4039	00010	0.0046	00010	0.0092	000010	0.0128
0011	0.0099	00011	0.0166	00011	0.0002	000011	0.0182
0100	0.4521	00100	0.0026	00100	0.3611	000100	0.0068
0101	0.0128	00101	0.0177	00101	0.0204	000101	0.0134
0110	0.0182	00110	0.0002	00110	0.0204	000110	0.0007
0111	0.0051	00111	0.0009	00111	0.0020	000111	0.0027

Continued on next page

Table I: Probabilities of each outcome in the implementation of Pessoa Júnior's circuit in a quantum hardware. This table includes less significant outcomes that are not shown in the histograms of Figure 11. (Continued)

Figure 11(a)		Figure 11(b)		Figure 11(c)		Figure 11(d)	
1000	0.0250	01000	0.4451	01000	0.4186	001000	0.0012
1001	0.0012	01001	0.0154	01001	0.0198	001001	0.0126
1010	0.0121	01010	0.0170	01010	0.0189	001010	0.0007
1011	0.0009	01011	0.0034	01011	0.0026	001011	0.0016
1100	0.0140	01100	0.0105	01100	0.0304	001100	0.0004
1101	0.0017	01101	0.0016	01101	0.0021	001101	0.0007
1110	0.0028	01110	0.0020	01110	0.0023	001110	0.0001
		01111	0.0004	01111	0.0007	001111	0.0002
		10000	0.0132	10000	0.0057	010000	0.3938
		10001	0.0175	10001	0.0005	010001	0.0239
		10010	0.0007	10010	0.0004	010010	0.0261
		10011	0.0018	10011	0.0001	010011	0.0051
		10100	0.0007	10100	0.0151	010100	0.0145
		10101	0.0007	10101	0.0013	010101	0.0016
		10110	0.0001	10110	0.0018	010110	0.0009
		11000	0.0211	10111	0.0002	010111	0.0001
		11001	0.0024	11000	0.0156	011000	0.0100
		11010	0.0005	11001	0.0028	011001	0.0038
		11011	0.0002	11010	0.0020	011010	0.0011
		11100	0.0011	11011	0.0002	011011	0.0005
		11101	0.0004	11100	0.0021	011100	0.0002
		11110	0.0001	11101	0.0007	011101	0.0001
		11111	0.0001	11110	0.0001	011110	0.0001
						100000	0.0094
						100001	0.0179
						100010	0.0015
						100011	0.0020
						100100	0.0001
						100101	0.0013
						100111	0.0001
						101000	0.0005
						101001	0.0010
						101010	0.0002
						101011	0.0002
						101100	0.0004
						101101	0.0001
						110000	0.0156
						110001	0.0022

Continued on next page

Table I: Probabilities of each outcome in the implementation of Pessoa Júnior's circuit in a quantum hardware. This table includes less significant outcomes that are not shown in the histograms of Figure 11. (Continued)

Figure 11(a)	Figure 11(b)	Figure 11(c)	Figure 11(d)	
			110010	0.0016
			110011	0.0005
			110100	0.0017
			110101	0.0001
			111000	0.0012
			111001	0.0002
			111100	0.0001
			111101	0.0001

Appendix E: Calibration data for the IBMQ quantum chips

The calibration data for the quantum chips used in our demonstrations are presented in Tables II and III.

ibm_sherbrooke parameters	Q0	Q1	Q2	Q3
Frequency (GHz)	4.63	4.74	4.82	4.75
T1 (μs)	504.54	403.20	250.71	410.81
T2 (μs)	153.58	320.04	203.46	323.55
Readout error (10^{-2})	1.074	3.857	2.612	4.545
Pauli-X error (10^{-4})	1.334	2.427	2.777	1.498
CNOT error (10^{-3})	-	1_0:5.238 1_2:6.291	-	3_2:7.291
Gate time (ns)	-	1_0:533.33 1_2:533.33	-	3_2:533.33

Table II: Calibration data for the IBMQ Eagle r3 processor ibm_sherbrooke quantum chip. The table only presents data relating to the qubits used in the simulation.

ibm_kyiv parameters	Q0	Q1	Q2	Q3
Frequency (GHz)	4.65	4.53	4.68	4.61
T1 (μs)	427.98	473.26	313.40	208.33
T2 (μs)	361.28	183.66	137.52	142.13
Readout error (10^{-2})	0.415	0.513	1.245	0.464
Pauli-X error (10^{-4})	0.991	1.426	6.860	2.134
CNOT error (10^{-3})	0_14:5.168 0_1:3.101	1_2:14.080	2_3:7.769	-
Gate time (ns)	0_14:561.78 0_1:561.78	1_2:561.78	2_3:561.78	-

Table III: Calibration data for the IBMQ Eagle r3 processor ibm_kyiv quantum chip. The table only presents data relating to the qubits used in the simulation.

[1] R. P. Feynman, Simulating physics with computers, Int J Theor Phys **21**, 6 (1982), doi: 10.1007/BF02650179.
[2] I. M. Georgescu, S. Ashhab, and F. Nori, Quantum simulation, Rev. Mod. Phys. **86**, 153 (2014), doi: 10.1103/RevModPhys.86.153.
[3] S. Lloyd, Universal Quantum Simulators, Science, **273**, 5278 (1996), doi: 10.1126/science.273.5278.1073.
[4] S. S. Gill et al., Quantum Computing: Vision and Challenges, http://arxiv.org/abs/2403.02240.

[5] Z. Zimborás et al., Myths around Quantum Computation before Full Fault Tolerance: What No-Go Theorems Rule out and What They Don't, doi: http://arxiv.org/abs/2501.05694.

[6] A. Macridin, A. C. Y. Li, S. Mrenna, and P. Spentzouris. 2022. Bosonic Field Digitization for Quantum Computers. Physical Review A **105**(5): 052405. doi:10.1103/PhysRevA.105.052405.

[7] R. D. Somma, Quantum Computation, Complexity, and Many-Body Physics, PhD thesis, Instituto Balseiro and Los Alamos National Laboratory (2005), doi: http://arxiv.org/abs/quant-ph/0512209.

[8] R. Bhowmick *et al.,* Towards Quantum Dynamics Simulation of Physical Systems: A Survey, doi: http://arxiv.org/abs/2310.11801.

[9] N. K. Mohan, R. Bhowmick, D. Kumar, and R. Chaurasiya, Digital Quantum Simulations of Hong-Ou-Mandel Interference, arXiv:2402.17522, doi: http://arxiv.org/abs/2402.17522.

[10] N. P. D. Sawaya, T. Menke, T. H. Kyaw *et al.*, Resource-efficient digital quantum simulation of d-level systems for photonic, vibrational, and spin-s Hamiltonians, npj Quantum Inf. **6**, 49 (2020), doi: 10.1038/s41534-020-0278-0.

[11] O. Di Matteo, A. McCoy, P. Gysbers *et al.*, Improving Hamiltonian encodings with the Gray code, Phys. Rev. A **103**, 042405 (2021), doi: 10.1103/PhysRevA.103.042405.

[12] N. Lorenzoni, T. Lacroix, J. Lim, D. Tamascelli, S. F. Huelga, and M. B. Plenio, Full Microscopic Simulations Uncover Persistent Quantum Effects in Primary Photosynthesis, doi: http://arxiv.org/abs/2503.17282.

[13] A. Baiardi, M. Christandl, M. Reiher, Quantum Computing for Molecular Biology, ChemBioChem **24**, e202300120 (2023), doi: 10.1002/cbic.202300120.

[14] J. Ye et al., Excitonic energy transfer in light-harvesting complexes in purple bacteria, J. Chem. Phys. **136**, 245104 (2012), doi: 10.1063/1.4729786.

[15] L. Xu et al., Differentiation of correlated fluctuations in site energy on excitation energy transfer in photosynthetic light-harvesting complexes, Results in Physics **38**, 105597 (2022), doi: 10.1016/j.rinp.2022.105597.

[16] D. G. A. Cabral et al., A Roadmap for Simulating Chemical Dynamics on a Parametrically Driven Bosonic Quantum Device, The Journal of Physical Chemistry Letters **15** (48), 12042-12050 (2024), doi: 10.1021/acs.jpclett.4c02864.

[17] S. Malpathak, S. D. Kallullathil, and A. F. Izmaylov, Simulating Vibrational Dynamics on Bosonic Quantum Devices, J. Phys. Chem. Lett. **16**, 1855 (2025), doi: 10.1021/acs.jpclett.4c03480.

[18] R. Dutta *et al.*, Simulating Chemistry on Bosonic Quantum Devices, J Chem Theory Comput **20**, 6426 (2024), doi: 10.1021/acs.jctc.4c00544.

[19] R. Dutta *et al.*, Simulating Electronic Structure on Bosonic Quantum Computers, Journal of Chemical Theory and Computation **21** (5), 2281-2300 (2025), doi: 10.1021/acs.jctc.4c01400.

[20] J. Leppäkangas *et al.*, Quantum simulation of the spin-boson model with a microwave circuit, Phys. Rev. A **97**, 052321 (2018), doi: 10.1103/PhysRevA.97.052321.

[21] A. Burger, L. C. Kwek, D. Poletti, Digital Quantum Simulation of the Spin-Boson Model under Markovian Open-System Dynamics, Entropy **24**(12), 1766 (2022), doi: 10.3390/e24121766.

[22] S. Kumar, N. N. Hegade, A.-M. Visuri, B. A. Bhargava, J. F. R. Hernandez, E. Solano, F. Albarrán-Arriagada, and G. A. Barrios, Digital-analog quantum computing of fermion-boson models in superconducting circuits, Npj Quantum Inf **11**, 1 (2025), doi: 10.1038/s41534-025-01001-4.

[23] A. Senanian et al., Programmable large-scale simulation of bosonic transport in optical synthetic frequency lattice, Nature Physics **19**, 1333-1339 (2023), doi: 10.1038/s41567-023-02075-7.

[24] A. Macridin et al., Digital quantum computation of fermion-boson interacting systems, Phys. Rev. A 98, 042312 (2018), doi: 10.1103/PhysRevA.98.042312.

[25] M. Tudorovskaya and D. M. Ramo, Quantum computing simulation of a mixed spin-boson Hamiltonian and its performance for a cavity quantum electrodynamics problem, Phys. Rev. A **109**, 032612 (2024), doi: 10.1103/PhysRevA.109.032612.

[26] C. Sabín, Digital Quantum Simulation of Linear and Nonlinear Optical Elements, Quantum Rep. **2**(1), 208-220 (2020), doi: 10.3390/quantum2010013.

[27] P. C. Encinar, A. Agustí, C. Sabín, Digital quantum simulation of beam splitters and squeezing with IBM quantum computers, Phys. Rev. A **104**, 052609 (2021), doi: 10.1103/PhysRevA.104.052609.

[28] J. A. Green and D. V. Shalashilin, Simulation of the quantum dynamics of indistinguishable bosons with the method of coupled coherent states, Phys. Rev. A **100**, 013607 (2019), doi: 10.1103/PhysRevA.100.013607.

[29] S. S. Afshar, E. Flores, K. F. McDonald, and E. Knoesel, Paradox in Wave-Particle Duality, Found Phys **37**, 295 (2007), doi: 10.1007/s10701-006-9102-8.

[30] Unruh, W. G., Quantum Rebel-S. Afshar, `https://archive.is/JgBtF`.

[31] O. Pessoa Júnior, Refinamentos da interpretação da complementaridade a partir do experimento de Afshar, Sci. stud. **11**, 119 (2013), doi: 10.1590/S1678-31662013000100006.

[32] The demonstrative results derived from IBM's quantum computers, which were utilized to generate the histograms and plots, can be accessed at: `https://github.com/victorpbrz/simulations-code/blob/main/digital_quantum_simulation/01-dqs_complementarity.ipynb`.

[33] C. C. Gerry and P. Knight, *Introductory Quantum Optics* (Cambridge University Press, Cambridge, UK; New York, 2005), doi: 10.1017/CBO9780511791239.

[34] Andrea Beggi *et al.*, Back and forth from Fock space to Hilbert space: a guide for commuters, Eur. J. Phys. **39** 065401 (2018), doi: 10.1088/1361-6404/aad760.

[35] N. Bohr, The Quantum Postulate and the Recent Development of Atomic Theory, Nature **121**, 580 (1928), doi: 10.1038/121580a0.

[36] M. L. W. Basso, D. S. S. Chrysosthemos, and J. Maziero, Quantitative Wave-Particle Duality Relations from the Density

Matrix Properties, Quantum Inf. Process. **19**, 254 (2020), doi: 10.1007/s11128-020-02753-y.
[37] D. S. Starke, M. L. W. Basso, and J. Maziero, An Updated Quantum Complementarity Principle, Proc. R. Soc. A **480**, 20240517 (2024), doi: 10.1098/rspa.2024.0517.
[38] T. Baumgratz, M. Cramer, and M. B. Plenio, Quantifying Coherence, Phys. Rev. Lett. **113**, 140401 (2014), doi: 10.1103/PhysRevLett.113.140401.
[39] S. Dürr, Quantitative wave-particle duality in multibeam interferometers, Phys. Rev. A **64**, 042113 (2001), doi: 10.1103/PhysRevA.64.042113.
[40] B. G. Englert, D. Kaszlikowski, L. C. Kwek, and W. H. Chee, Wave-particle duality in multi-path interferometers: General concepts and three-path interferometers, Int. J. Quant. Inf. **6**, 129 (2008), doi: 10.1142/S0219749908003220.
[41] M. L. W. Basso and J. Maziero, Complete Complementarity Relations for Multipartite Pure States, J. Phys. A: Math. Theor. **53**, 465301 (2020), doi: 10.1088/1751-8121/abc361.
[42] M. L. W. Basso and J. Maziero, Entanglement Monotones from Complementarity Relations, J. Phys. A: Math. Theor. **55** 355304 (2022), doi: 10.1088/1751-8121/ac83fc.
[43] M. Jakob and J. Bergou, Quantitative complementarity relations in bipartite systems: Entanglement as a physical reality, Opt. Comm. **283**, 827 (2010), doi: 10.1016/j.optcom.2009.10.044.
[44] M. Jakob and J. Bergou, Generalized Complementarity Relations in Composite Quantum Systems of Arbitrary Dimensions, Int. J. Mod. Phys. B **20**, (2012), doi: 10.1142/S0217979206033851.
[45] A. K. Roy, N. Pathania, N. K. Chandra, P. K. Panigrahi, and T. Qureshi, Coherence, path predictability, and I concurrence: A triality, Phys. Rev. A **105**, 032209 (2022), doi: 10.1103/PhysRevA.105.032209.
[46] C. Dittel, G. Dufour, G. Weihs, and A. Buchleitner, Wave-particle duality of many-body quantum states, Phys. Rev. X **11**, 031041 (2021), doi: 10.1103/PhysRevX.11.031041.
[47] D. M. Greenberger and A. Yasin, Simultaneous Wave and Particle Knowledge in a Neutron Interferometer, Phys. Let. A **128**, 391 (1988), doi: 10.1016/0375-9601(88)90114-4.
[48] D. S. S. Chrysosthemos, M. L. W. Basso, and J. Maziero, Quantum Coherence versus Interferometric Visibility in a Biased Mach–Zehnder Interferometer, Quantum Inf. Process. **22**, 68 (2023), doi: 10.2139/ssrn.4234350.
[49] Y. Maleki and M. S. Zubairy, Revisiting wave-particle duality in Bohr-Einstein debate, AVS Quantum Science **5**, 031401 (2023), doi: 10.1116/5.0148225.
[50] W. G. Unruh, Comment on "Single Photon Experiments and Quantum Complementarity"; by D. Georgiev, Progress in Physics 2007, **27** (2007).
[51] R. E. Kastner, Why the Afshar experiment does not refute complementarity, Studies in History and Philosophy of Science Part B: Studies in History and Philosophy of Modern Physics **36**, 649 (2005), doi: 10.1016/j.shpsb.2005.04.006.
[52] E. Flores and E. Knoesel, Why Kastner Analysis Does Not Apply to a Modified Afshar Experiment, in The Nature of Light: What Are Photons?, Vol. **6664** (SPIE, 2007), pp. 220-227, doi: 10.1117/12.730965.
[53] O. Steuernagel, Afshar's Experiment Does Not Show a Violation of Complementarity, Found Phys **37**, 1370 (2007), doi: 10.1007/s10701-007-9153-5.
[54] D. D. Georgiev, Single Photon Experiments and Quantum Complementarity, Prog. Phys. **2**, 97 (2007).
[55] D. D. Georgiev, Exact Mapping of Quantum Waves between Unruh's and Afshar's Setup (Reply to W. Unruh), Prog. Phys. **3**, 28 (2007).
[56] E. V. Flores, Reply to Comments of Steuernagel on the Afshar's Experiment, Found Phys **38**, 778 (2008), doi: 10.1007/s10701-008-9234-0.
[57] A. Drezet, Wave particle duality and the Afshar experiment, Prog. Phys. **1**, 57 (2011).
[58] T. Qureshi, Modified Two-Slit Experiments and Complementarity, JQIS **02**, 35 (2012), doi: 10.4236/jqis.2012.22007.
[59] B. Gergely and H. Batelaan, Simulation of Afshar's Double Slit Experiment, Found Phys **52**, 69 (2022), doi: 10.1007/s10701-022-00585-7.
[60] J. A. Wheeler, *Quantum Theory and Measurement*, edited by J. A. Wheeler and W. H. Zurek (Princeton University Press, Princeton, NJ, 1984), ISBN: 9780691641027.
[61] J. Flórez, N. J. Carlson, C. H. Nacke, L. Giner, and J. S. Lundeen, A Variable Partially-Polarizing Beam Splitter, Review of Scientific Instruments **89**, 023108 (2018), doi: 10.1063/1.5004805.
[62] S. P. Walborn, P. H. Souto Ribeiro, L. Davidovich, F. Mintert, and A. Buchleitner, Experimental Determination of Entanglement with a Single Measurement, Nature **440**, 1022 (2006), doi: 10.1038/nature04627.
[63] A. C. Elitzur and L. Vaidman, Quantum mechanical interaction-free measurements, Found Phys **23**, 987 (1993), doi: 10.1007/BF00736012.
[64] R. Chaves, G. B. Lemos, and J. Pienaar, Causal Modeling the Delayed-Choice Experiment, Phys. Rev. Lett. **120**, 190401 (2018), doi: 10.1103/PhysRevLett.120.190401.